MSUCP-33
June 1980

THE EXTRACTION SYSTEM FOR THE K-500 CYCLOTRON AT MSU

E. Fabrici, D. Johnson, F.G. Resmini
Michigan State University, East Lansing, Michigan 48824

ABSTRACT

The final design features of the extraction system for the K-500 cyclotron under construction at MSU are presented. The resulting cyclotron performance for a number of typical ions are reviewed and the expected extracted beam phase space characteristics are also discussed.

1. Introduction

This paper reports the final design features of the K–500 cyclotron extraction system, under construction at MSU, as of March 1980. It differs in several aspects, especially construction-wise, from schemes reported earlier[1] and it seems worthwhile to review in some detail the rationale for the present choices and the expected performances.

As described in [1] the system consists of electrostatic deflectors, followed by several magnetic channels of the passive type i.e. made with bars of saturated iron. The main changes introduced are:

- all elements, i.e. deflectors and channels, are radially movable.
- the number of electrostatic deflectors has been reduced from three to two.
- the number of magnetic channels has been increased to eight.
- a magnetic channel has been inserted in the traversal of the yoke.

These modifications stemmed out of a careful analysis of the internal and extracted beam dynamics for several representative ions which cover the entire operating range of the cyclotron. Realistic field maps, with properly isochronized fields as described in [2], were used throughout. Since detailed studies of the internal beam dynamics are reported elsewhere[3], we shall only concern ourselves here with the characteristics and performance of the extraction system itself.

2. Layout and design features

The pole tip geometry, together with the layout of the extraction system, is schematically presented in Fig. 1. Shown are the hills contours, including the hill shoe, 60° wide, and positioned in the inner tank wall from 26" to 27" in radius.[2] All the azimuths referred to in this paper are according to the scale of Fig. 1.

We shall first give a general description of the extraction scheme, analyzing later in detail the single components.

a-Main characterists

All the elements shown in Fig. 1 are also listed in Table I together with their main parameters. The entries in Table I are as follows:

E, M, C = characterizes an electrostatic deflector, a magnetic channel or a compensating bar respectively.

θ_I, θ_F = initial and final azimuth of the element as referred to in Fig. 1.

$\bar{R}_I$, $\bar{R}_F$ = average central ray radius at the initial and final azimuth of each element.

ΔR = range of radial movement for each element around the average position.

E_{max}, B, $\frac{\partial B}{\partial x}$ = maximum electric field for deflectors, bias magnetic field and gradient for the magnetic channels.

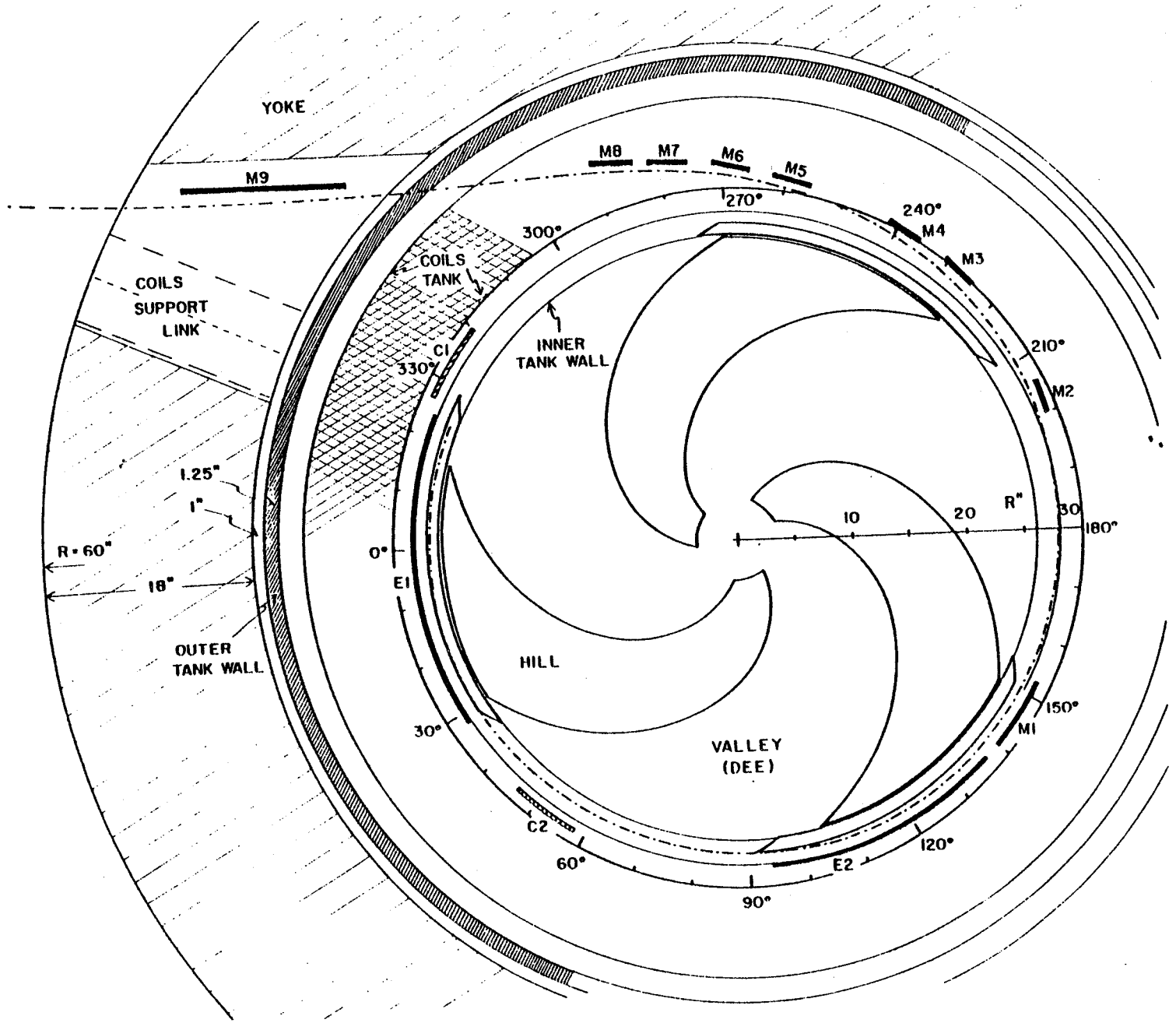

FIG. 1. Median plane cross section of the K-500 cyclotron together with the extraction scheme.

Table I. Extraction elements parameters.

	θ_I	θ_F	$\bar{R}''_I$	$\bar{R}''_F$	$\Delta R''$	E_{max}	B	$\frac{\partial B}{\partial x}$
	(Deg.)					(kV/cm)	(kG)	(kG/inch)
E_1	-23.	32.	26.59	26.93	±.17	133	--	--
E_2	94.	137.	27.10	27.68	±.23	132	--	--
M_1	140.	153.	27.70	27.76	±.18	--	-1.2	8.8
M_2	200.	206.	28.28	28.39	±.24	--	-1.2	8.8
M_3	226.	232.	28.89	29.08	±.20	--	-1.2	8.8
M_4	236.	242.	29.21	29.44	±.16	--	-1.2	8.8
M_5	256.	262.	30.09	30.46	±.09	--	-1.2	8.8
M_6	266.	272.	30.75	31.24	±.06	--	-1.2	8.8
M_7	276.	282.	31.62	32.31	±.12	--	-1.2	8.8
M_8	286.	292.	32.88	33.95	±.26	--	-1.2	8.8
C_1	320.	334.	27.75	27.75	±.10	--	--	--
C_2	46.	58.	28.95	28.95	±.25	--	--	--

Two electrostatic deflectors, the first one 55^o long, and the second 43^o long, are positioned in correspondence of two successive hills, the extracted rays being inside the dee in between. They are followed by eight magnetic channels, the first of which is 13^o long and is adjacent to the second deflector. The need for having this radially focusing element immediately after the deflector is supported by a number of phase space trackings of extracted beams, and is the reason for the reduced length of the second deflector. The other seven channels are 6^o long each, and after M_5 are regularly spaced along the extraction path. The large azimuthal clearance

between M_4 and M_5, 14^o, will allow space for the insertion of a beam probe. The extracted beam is well outside the dee which follows the second deflector, and M_2 starts close to the end of that dee. The spacing between M_2 and M_3 is needed because of the presence of the radial coils support link (these are three of them, 120^o apart, one only being sketched in Fig. 1.)

Other two elements can be noted in Fig. 1, namely the compensating bars C_1 and C_2. The first one compensates the field perturbation on the inner orbits due to M_1, and is therefore at 180^o from the latter. The second compensates the overall effect of the seven remaining channels. A detailed analysis of the compensating effects in terms of first and second harmonics is given in [3].

The azimuthal length of the extraction path, form the entrance of the first deflector to the exit of the outer tank wall, is 331^o. The traversal of the yoke will be described later.

All elements are radially movable, typically by $\pm$ .25" around a center position. The average central-ray values of the entrance and exit of each element, and which correspond therefore to the center line of either a deflector or a magnetic channel are listed in Table I, together with the required displacements. The latter are not the same for every element, but they have been set to the maximum ($\pm$ .25") in order to standardize the mechanical design. The need for the radial movement stems out of the following points:

- the shape of the average fields in the fringing region varies considerably from ion to ion, as reported in [2], and so does the ν_R vs R curve for each ion,(3) which determines to a large extent the extraction radius.
- the need to avoid the $\nu_R + 2\,\nu_Z = 3$ resonance(2,3) forces to extract at inner radii at low average fields. More external radii are instead possible for the high field cases, thus easing the requirements on electric fields.
- while it is not altogether excluded that by adjusting the electric fields one may be able to steer the extracted trajectories along a fixed common path, this looks difficult because both of the number of elements and the large variations in orbit scalloping across the anticipated range of magnetic fields.

b-The extraction elements

As an example a view of the 2nd deflector is shown in Fig. 2. The high voltage electrode is supported by three insulators, and a vertical cross section at the location of one of the insulators is shown in Fig. 3. A box-like construction is adopted for the deflector, the whole system being moved radially by two actuators as indicated in Fig. 2 and shown in a cross-section by Fig. 4. The gap is set fixed to 8 mm which, at the maximum electric field of 133 kV/cm listed in Table I, corresponds to a voltage of 106 kV. The relevant VE number of $1.41\ 10^4$ should not pose particular problems. The high voltage is brought in via a feed-through as shown by the cross section of Fig. 5.

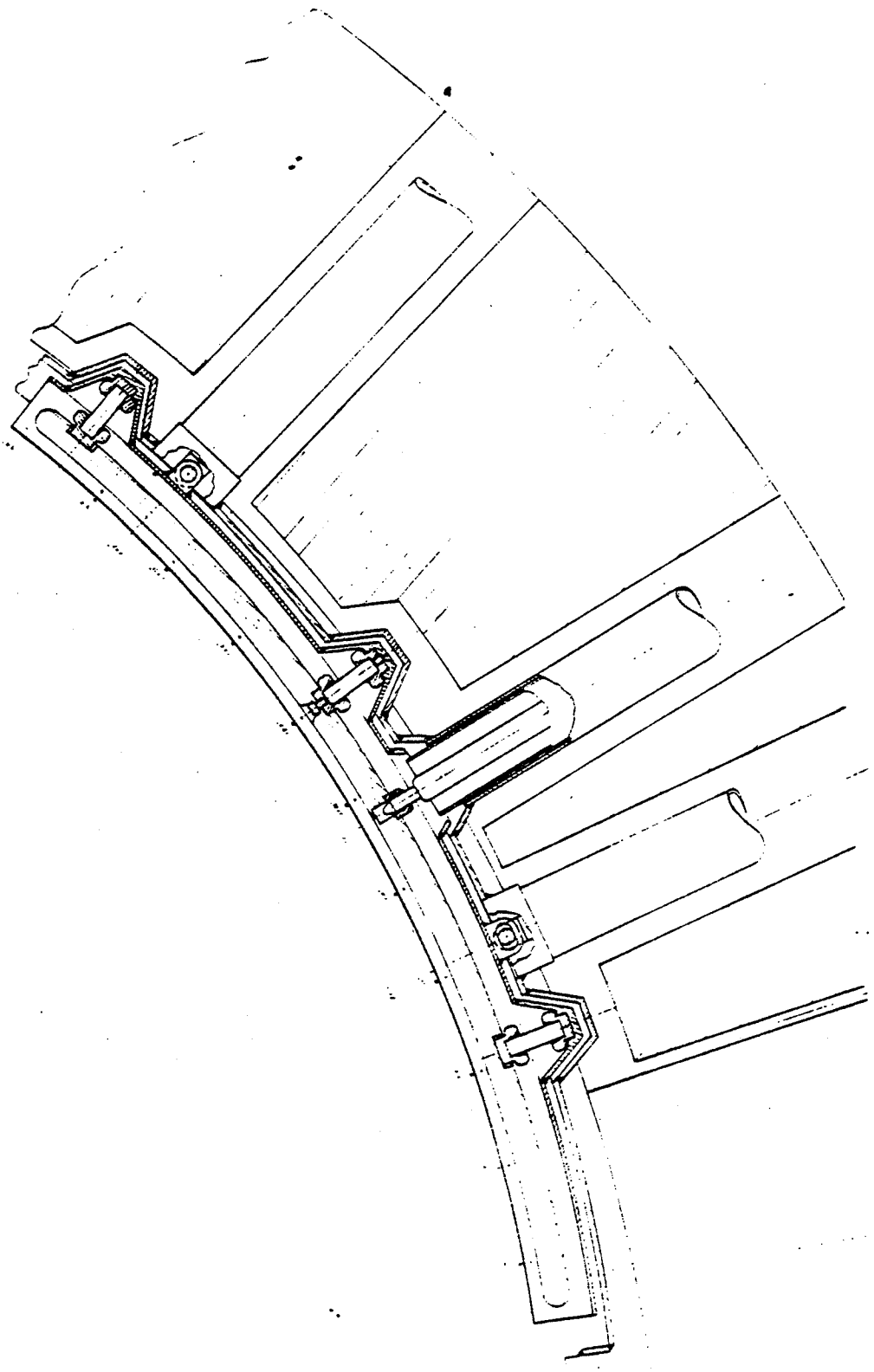

FIG. 2. View of the second electrostatic deflector.

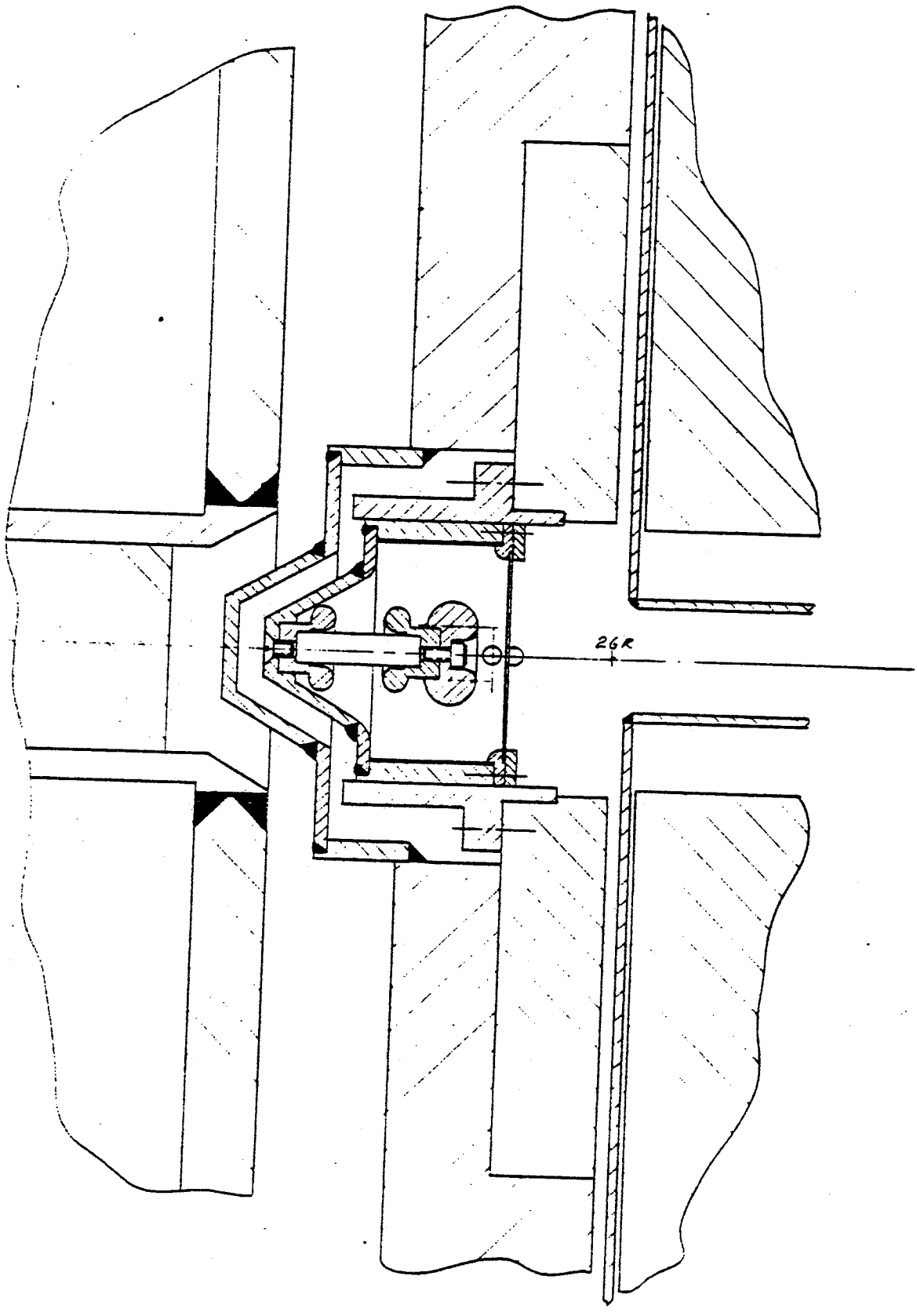

FIG. 3. Vertical cross section at the location of one of the insulators. The dots mark the minimum and the maximum beam positions.

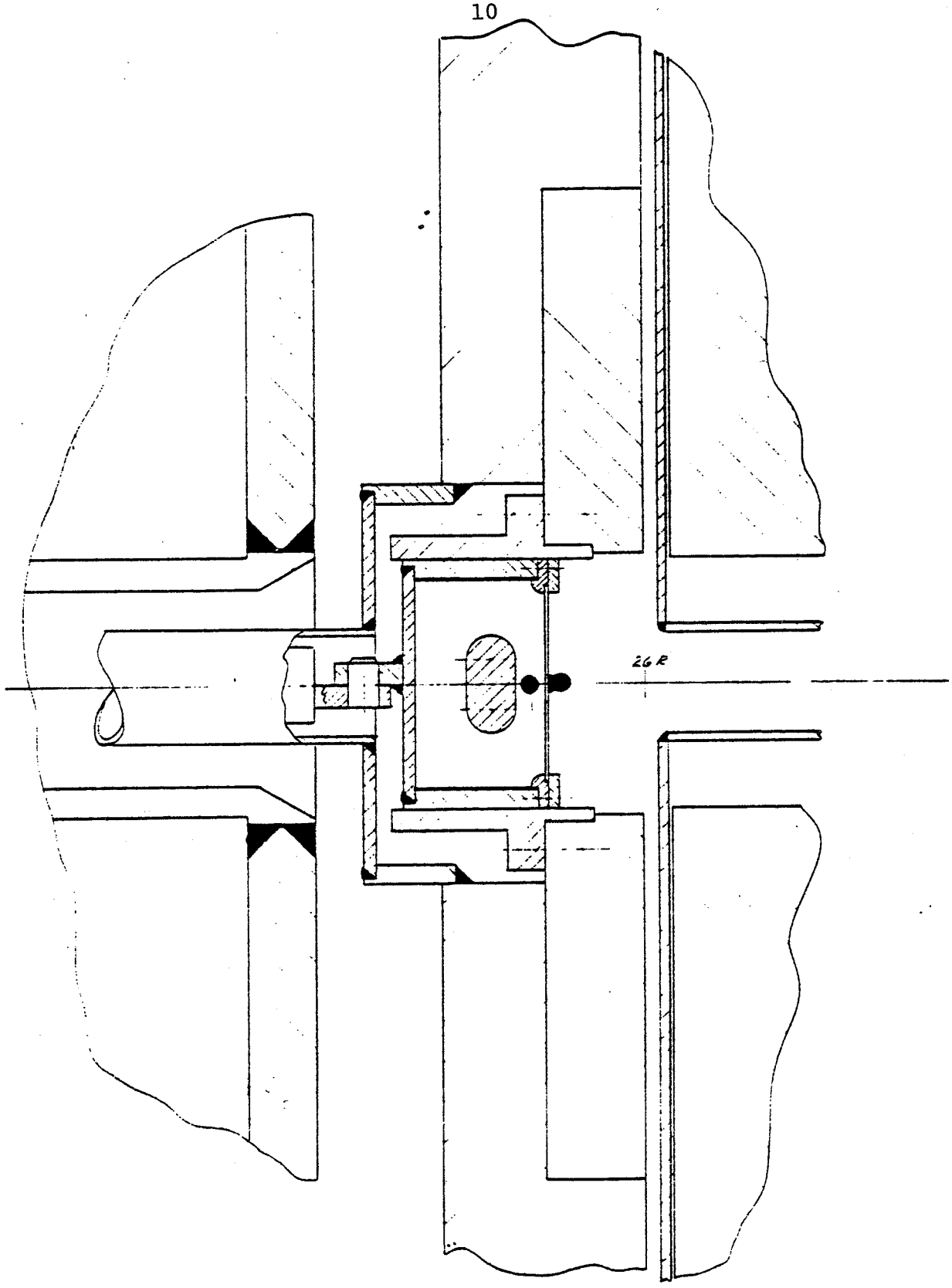

25°

FIG. 4. Vertical cross section at the location of one of the actuators. The dots mark the minimum and the maximum beam positions.

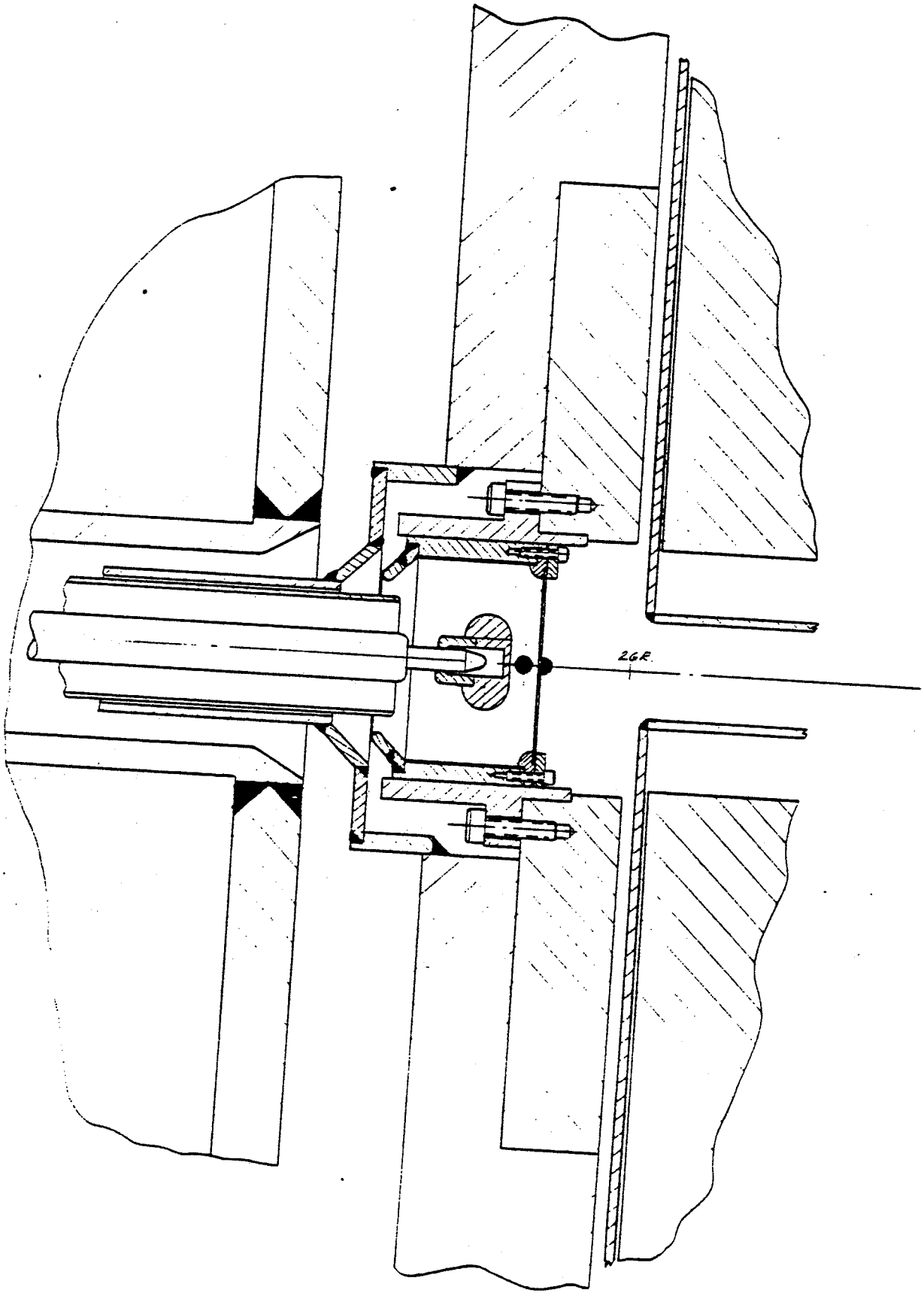

7.

FIG. 5. Vertical cross section at the location of the high voltage feed-through of the 1st electrostatic deflector. The dots mark the minimum and the maximum beam positions.

A schematic cross section of the magnetic channels, which are all of the same type, is shown in Fig. 6, together with a plot of the field and the radial gradient $\frac{\partial B}{\partial x}$ across the channel itself. The latter are results of calculations based on the hypothesis of uniform saturation of the three bars which constitute the channel. As listed in Table I, each channel provides a negative field bias of 1.2 kgauss, thus easing the extraction, and a gradient of 8.8 kgauss/inch. The latter, as shown in Fig. 6, is constant within $\pm$ 5% across the beam width ($\pm$ .15" at most) and is therefore quite adequate.

A more detailed cross section of one of the channels, in this case M_2 at $\theta=203^{\circ}$, is shown in Fig. 7. The channels are radially moved via actuators as shown in Fig. 8. Rectangular holes both in the cryostat and the yoke allow the insertion and removal of the channels from the outside. The only exception is channel M_1, which has to be mounted from the inside, just like the deflectors. The relative small azimuthal length of the channels, i.e. 6°, has been selected for construction reasons. Longer channels would be impractical, because the compression forces exerted by the coils would be difficult to withstand across azimuthally larger holes in the cryostat.

As for the compensating bars C_1 and C_2, their relevant dimensions are shown in Figs. 9 and 10 respectively. These bars, whose position is quite apparent in Fig. 1, will also be mounted from the inside, and will be radially movable via actuators similar to those used for the channels. A cross

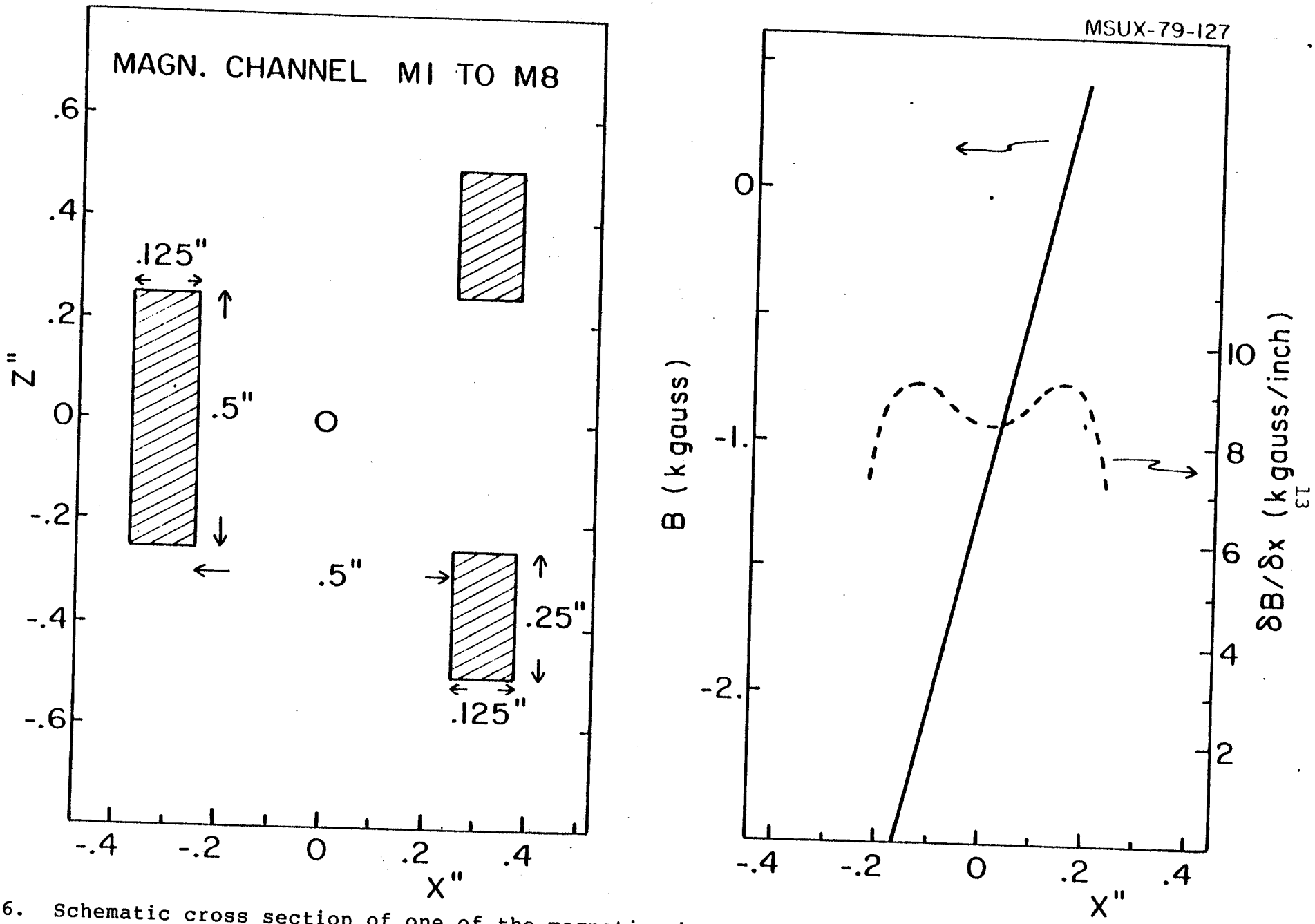

FIG. 6. Schematic cross section of one of the magnetic channels (left). The dot in the middle marks the beam position. The right presents the field and the gradient across the channel.

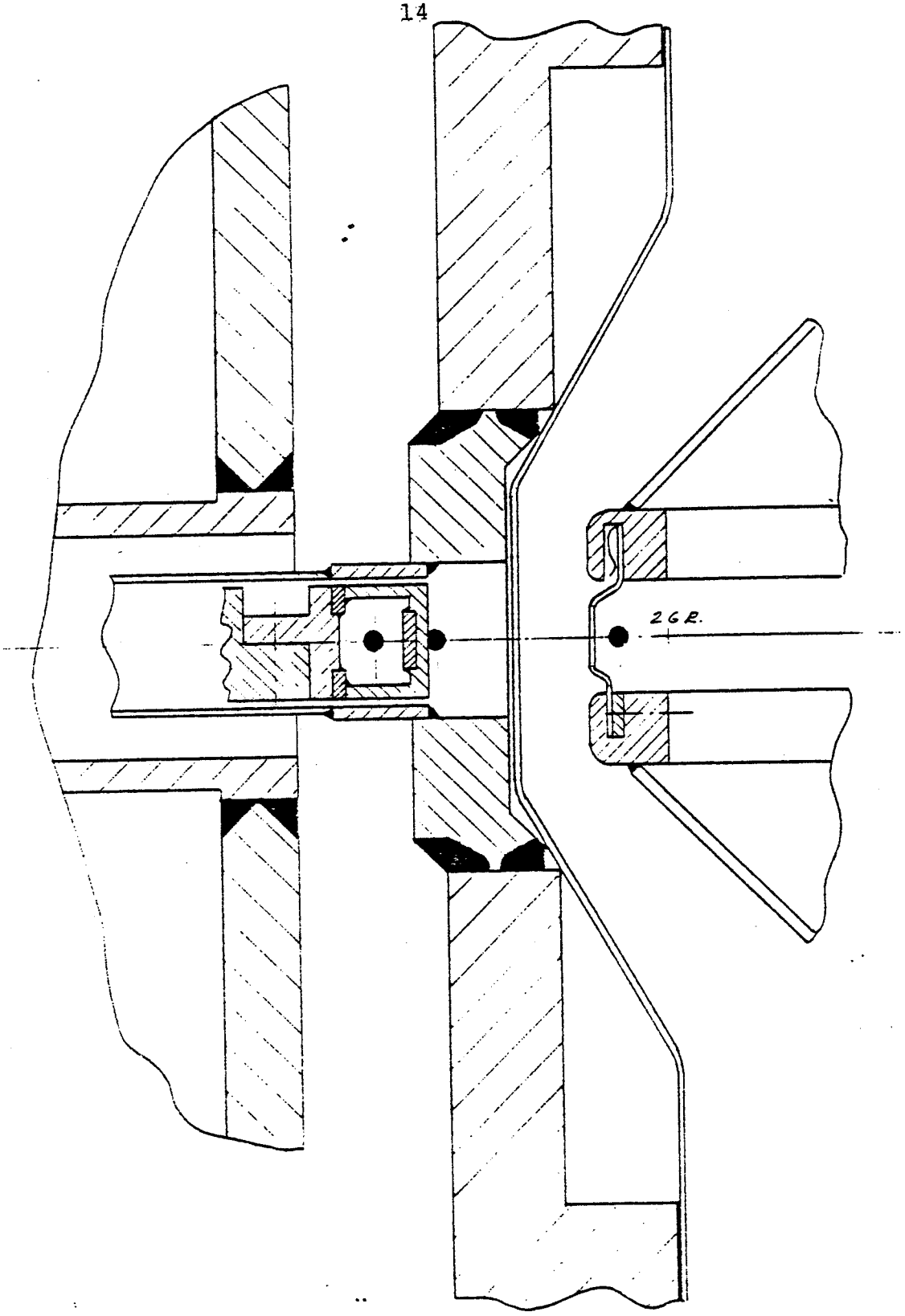

203°

FIG. 7. Vertical cross section of one of the magnetic channels (M_2 at θ=203°). The dots mark the minimum and the maximum positions of the extracted beams (left) and the last accelerated orbit (right).

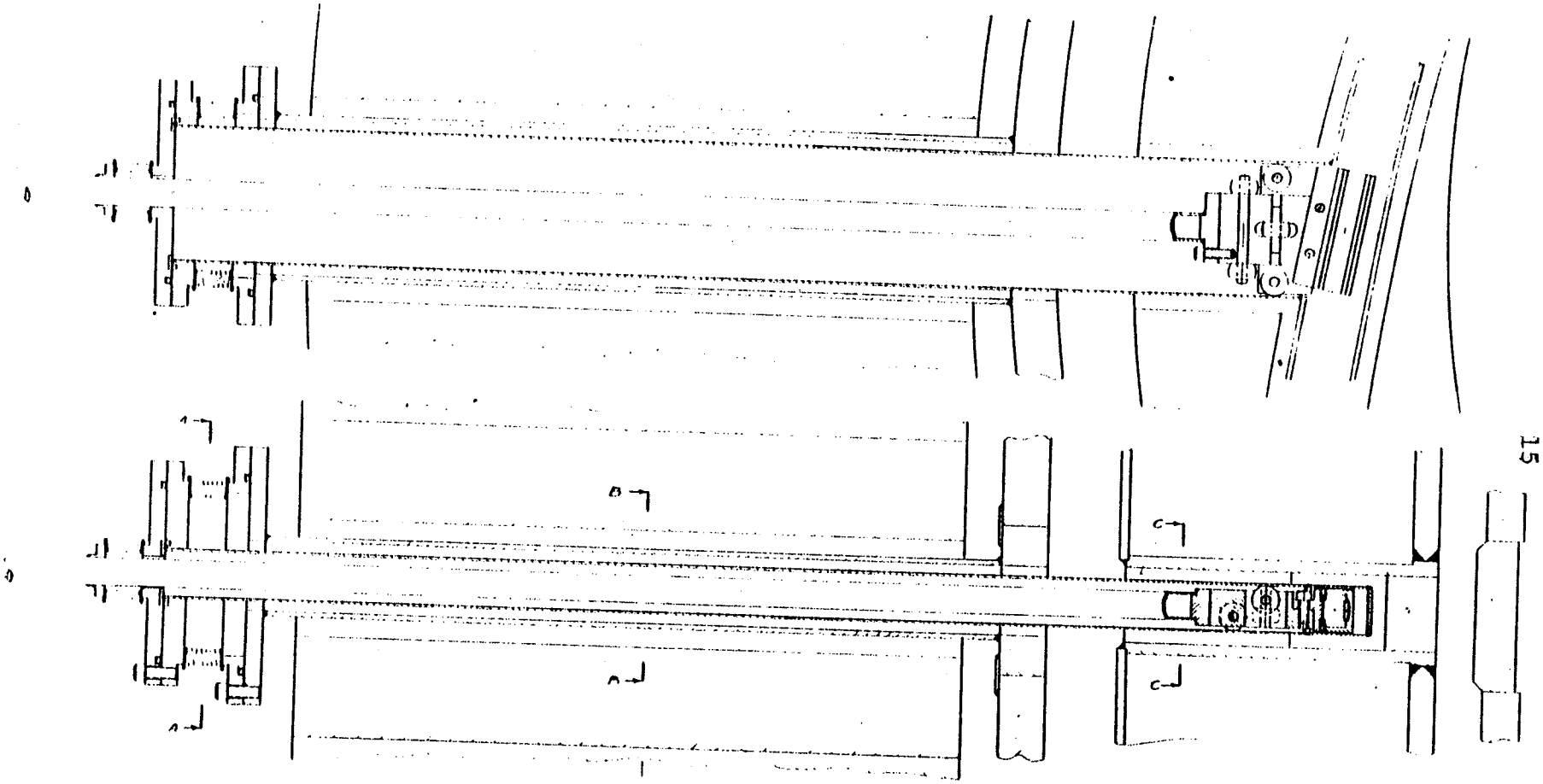

FIG. 8. Top view of one of the magnetic channel actulators (upper) and vertical cross section of the same (lower).

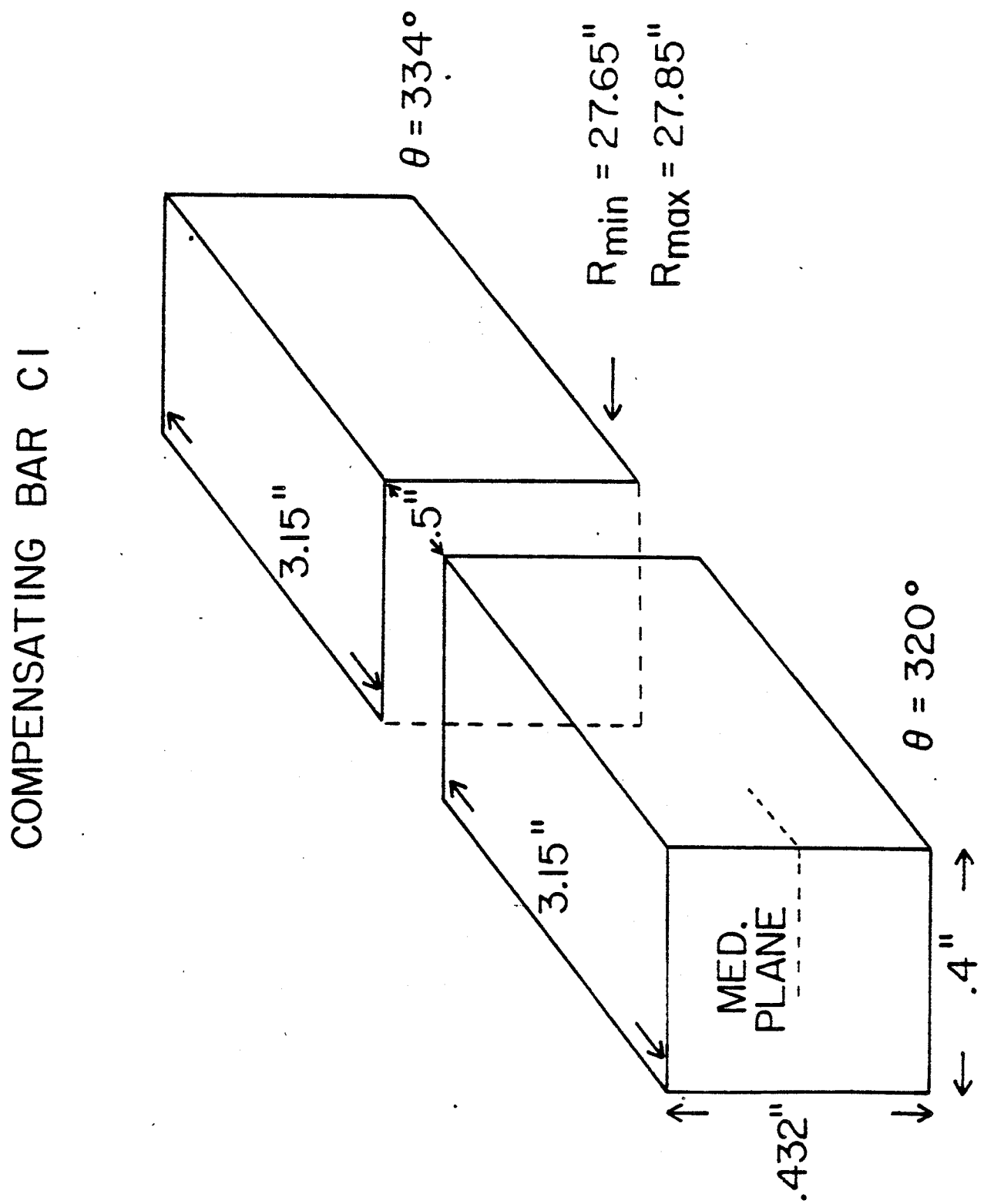

FIG. 9. Schematic view of the compensating bar C_1.

MSUX-79-124

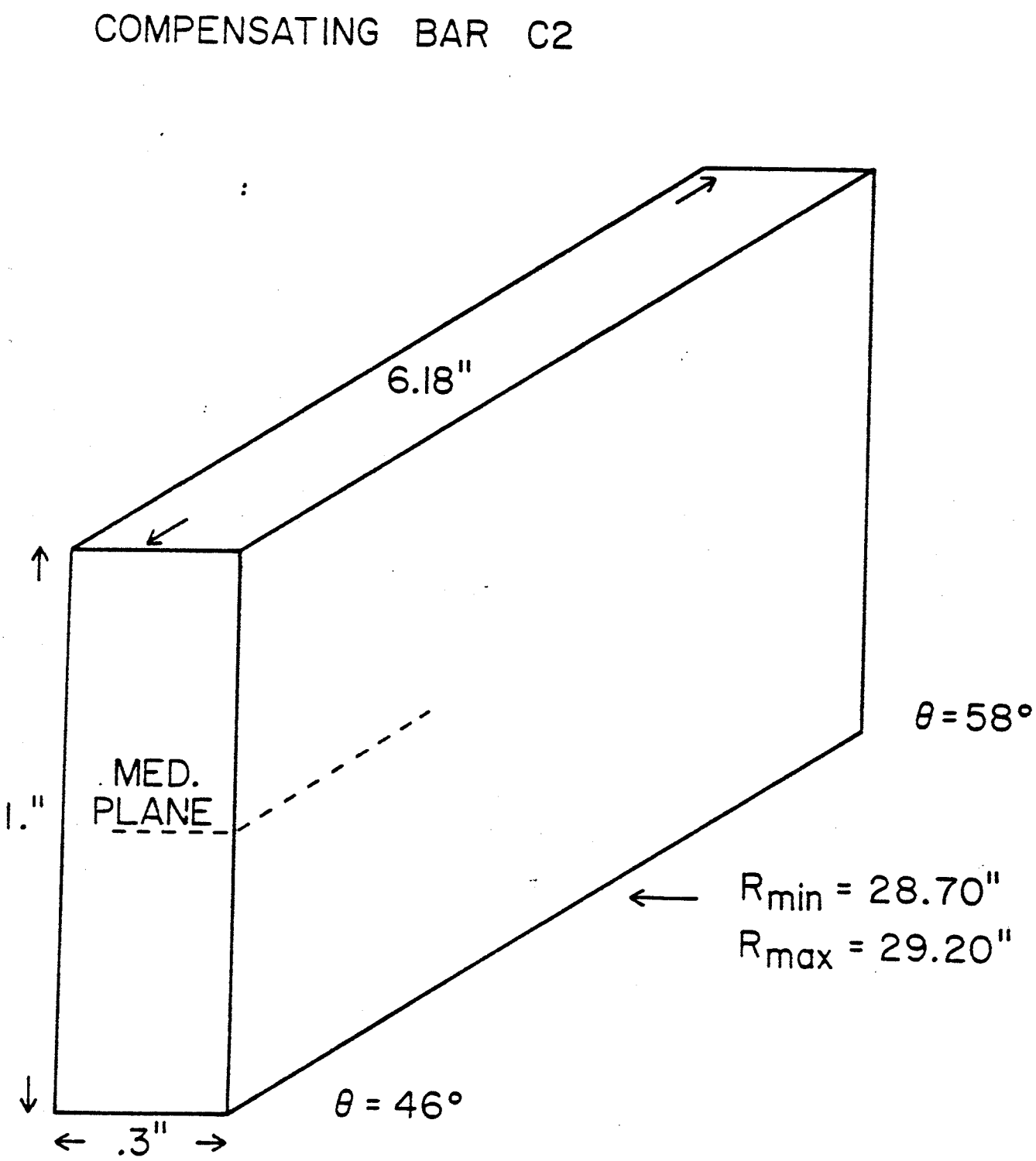

FIG. 10. Schematic view of the compensating bar C_2.

section of C_2 at $\theta=52^o$ is shown as an example in Fig. 11. The solid and dashed lines represent the maximum and minimum radial positions of the bar itself.

A number of radial holes must therefore be drilled in the yoke for accomodating the channels, voltage feedthroughs, actuators etc. These holes, because of their highly asymmetric position, as shown in Fig. 12, give rise to a first and second harmonic perturbation which may be as high as 20 and 30 gauss respectively near the radius where $\nu_R=1$. Compensation of such harmonics is therefore mandatory. This was done by drilling in the yoke three additional holes which are also shown in Fig. 12. One of the holes, compensates for the 1^{st} harmonics, while the two others, being 180^o apart, compensate for the second. When such a scheme is adopted the resulting first harmonic from the yoke is down to less than a gauss, the second to 5-6 gauss.

3. Performances

The analysis of the performances of the extraction system, and indeed the iterative optimization which led to this design, has been made by choosing eight representative ions. These notations are used in the following:

- Z/A = charge to mass ratio of a given ion;
- B_o = center field value in kgauss for which the isochronous field is computed;
- T/A= energy of the ion in MeV/nucleon.

In the (B_o,Z/A) plane, the operating diagram of the K-500 cyclotron is shown in Fig. 13, together with constant T/A

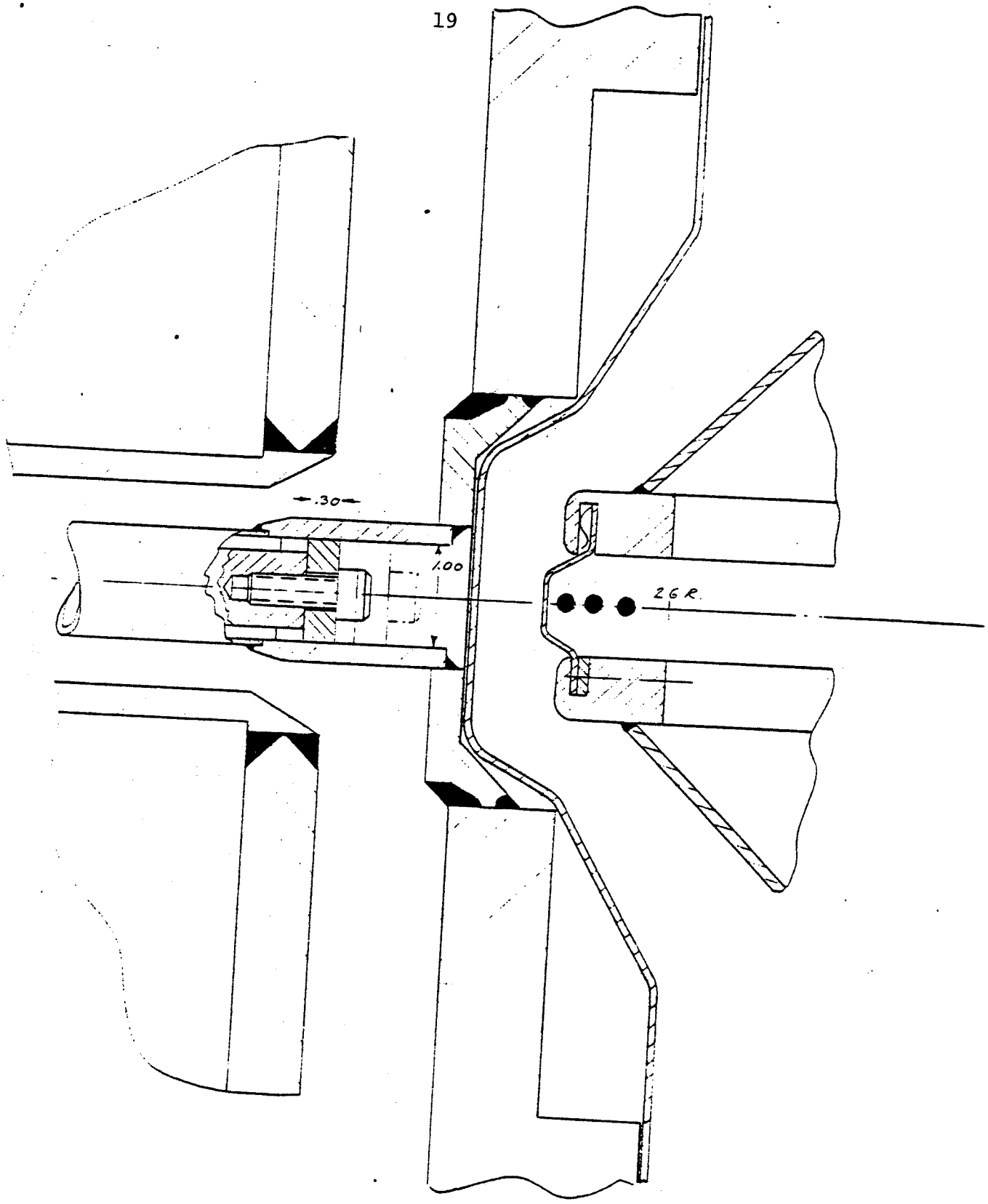

52

FIG. 11. Vertical cross section of the compensating bar C_2. Solid and dashed lines represent the maximum and the minimum radial position of the bar itself.

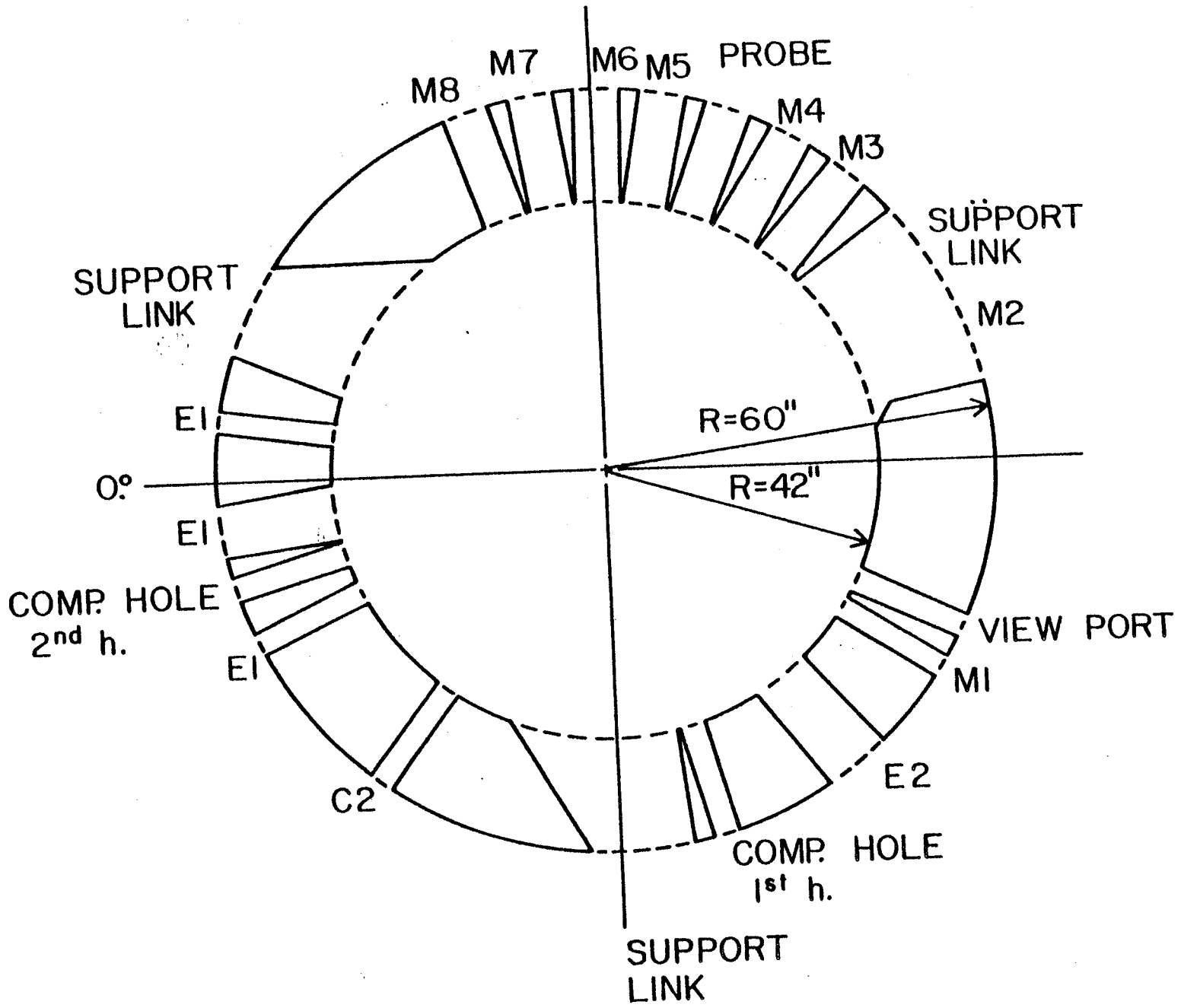

FIG. 12. Median plane section of the yoke showing the holes for accomodating the elements of the extraction system.

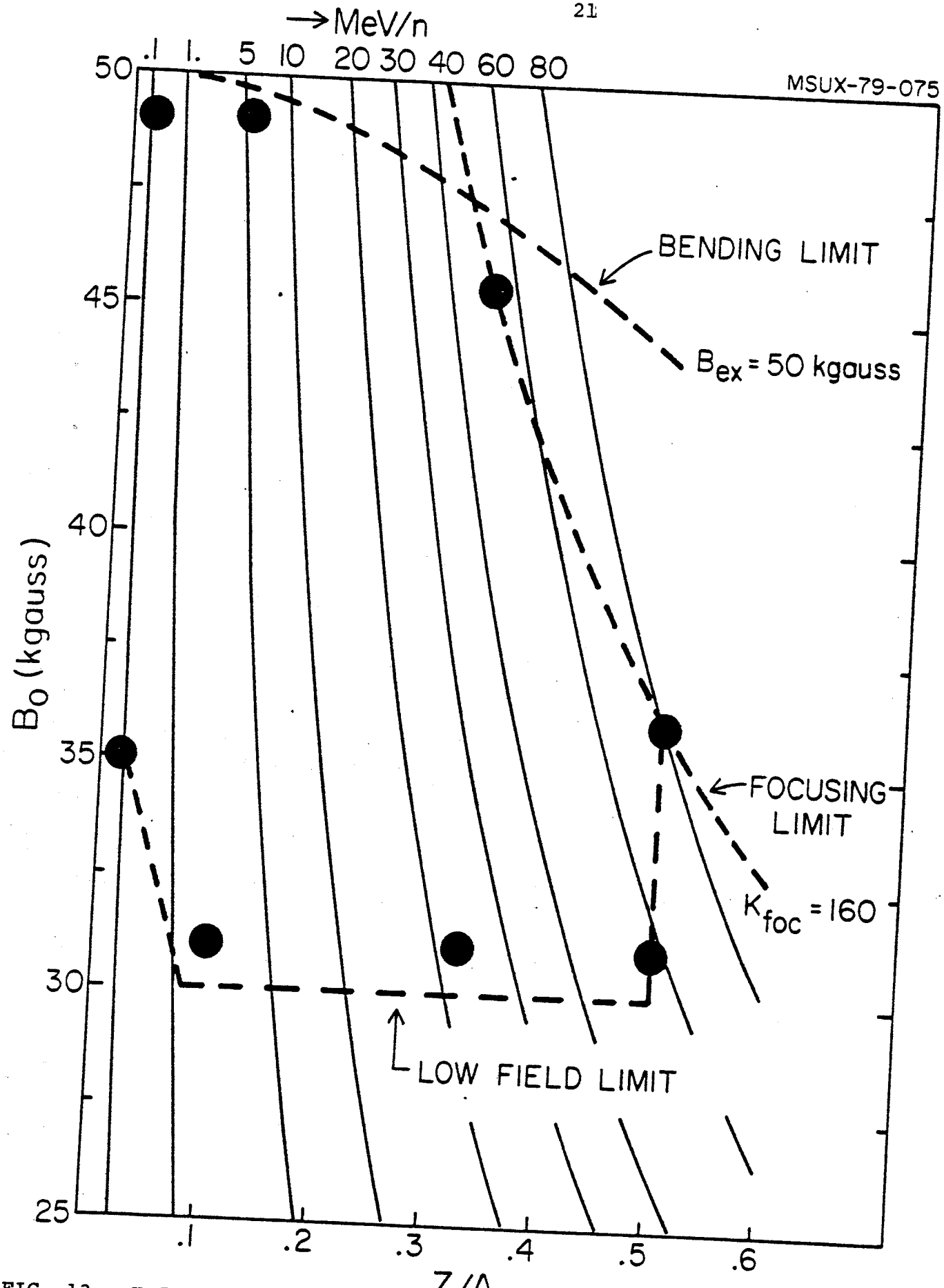

FIG. 13. K-500 operating diagram in the (Bo,Z/A) plane. Constant T/A lines are also shown. The dots indicate the representative ions for this study.

lines. The diagram is bounded by the K=500 bending limit, i.e. 50 kgauss at extraction radius, the focusing limit, and the low field limit of $B_o \approx 30$ kgauss discussed in [3]. Basically the K-500 will operate as stand-alone machine for the range $.1 \leq Z/A \leq .5$, while as injector for the planned K-800 cyclotron[4] just the range $Z/A \leq .15$, i.e. rather low energies, will be used.

The eight ions chosen are shown by dots in Fig. 13, and their parameters listed in Table II. They correspond to four different charge to mass ratios, i.e. Z/A = .02, .1, .322, .5, and for each one both the maximum and minimum B_o values are considered. The two cases with smaller Z/A are obviously injector-mode ions.

Table II. Representative ions used for this study.

Z/A	B_o (kgauss)	$T/A_{extr.}$ (MeV/n)
.02	49.0	.206
.02	35.0	.106
.1	49.0	5.16
.1	31.0	2.08
.322	45.5	49.87
.322	31.0	22.20
.5	36.0	79.50
.5	31.0	56.17

For these eight ions, the central radii at the entrance of each element are listed in Table III together with the electric fields on each deflector.

On a cartesian (R,θ) plot, the trajectories of four of the ions, i.e. those with highest and smallest Z/A, are shown in Fig. 14, up to the azimuthal position of the fifth magnetic channel. The effects of the different scalloping of the orbits are quite evident. It is apparent from Table III that the highest electric field, 133 kV/cm, is needed for the ion with Z/A = .322 and B_o = 45.5 kgauss. As it can be seen from Fig. 13, the latter is at the crossing of the K=500 and K_{FOC} =160 lines and the result is therefore not surprising. The fact that for Z/A=.5 the ion requiring a slightly higher electric field has the lower B_o value, i.e. 31 kgauss, is due to the more internal extraction radius, which is in turn due to the presence of the $\nu_R + 2\nu_Z = 3$ resonance at low fields. As listed in Table III, all ions have different radii at $\theta=308^o$, which corresponds roughly to the exit from the outer tank wall, R∿40". Different radii are also apparent at $\theta=330^o$ which for a radius of 60" corresponds to the exit from the yoke. All trajectories have however the same 69" radius at $\theta=334^o$ because the electric fields in the second deflector were so chosen as to have all rays passing through a common point just outside the yoke. However the beam behaviour in this region, i.e. between 40" and 60" in radius, will be discussed later in some detail.

The radial and axial beam envelopes for all eight ions are presented in Figs. 15 to 22. The initial phase space

Table III. Electric fields and central ray data for eight representative ions.

Extr. Element \ $Z/A/B_o$		.02/49	.02/35	.1/49	.1/31	.322/45.5	.322/31	.5/36	.5/31
E_1	R"(-23°)	26.51	26.50	26.54	26.51	26.61	26.46	26.73	26.51
	E(kV/cm)	4.82	1.90	45.7	9.20	133.	60.50	129.0	131.75
E_2	R"(94°)	27.06	26.87	27.02	26.99	27.30	27.09	27.33	27.13
	E(kV/cm)	4.958	1.241	45.04	4.302	130.99	60.817	128.38	131.98
M_1	R"(140°)	27.64	27.54	27.63	27.62	27.84	27.71	27.85	27.75
M_2	R"(200°)	28.28	28.04	28.34	28.05	28.51	28.26	28.45	28.38
M_3	R"(226°)	28.90	28.70	28.95	28.71	29.08	28.89	29.03	28.99
M_4	R"(236°)	29.22	29.05	29.26	29.07	29.37	29.22	29.32	29.31
M_5	R"(256°)	30.10	30.01	30.12	30.02	30.18	30.11	30.14	30.18
M_6	R"(266°)	30.73	30.69	30.73	30.71	30.76	30.77	30.72	30.81
M_7	R"(276°)	31.59	31.63	31.56	31.66	31.56	31.68	31.54	31.69
M_8	R"(286°)	32.81	32.97	32.76	33.05	32.72	33.00	32.73	32.98
M_8	R"(308°)	38.51	39.28	38.36	39.59	38.29	39.40	38.59	39.32
M_8	R"(330°)	59.13	60.29	59.00	60.70	59.05	60.50	59.73	60.44
M_8	R"(334°)	69.00	69.00	69.00	69.00	69.00	69.00	69.00	69.00

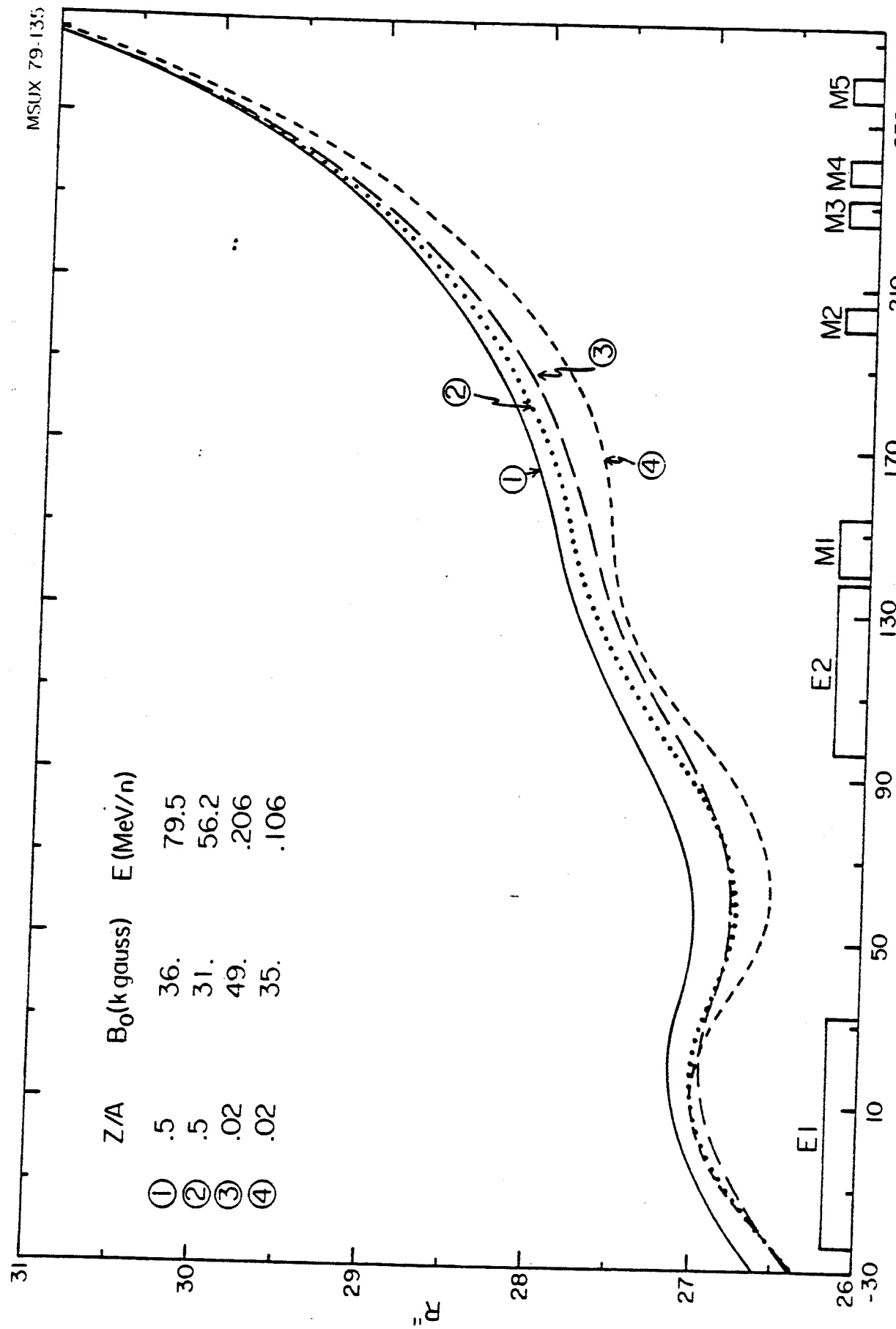

FIG. 14. Extraction trajectories of four of the investigated ions on a cartesian (R,θ) plot.

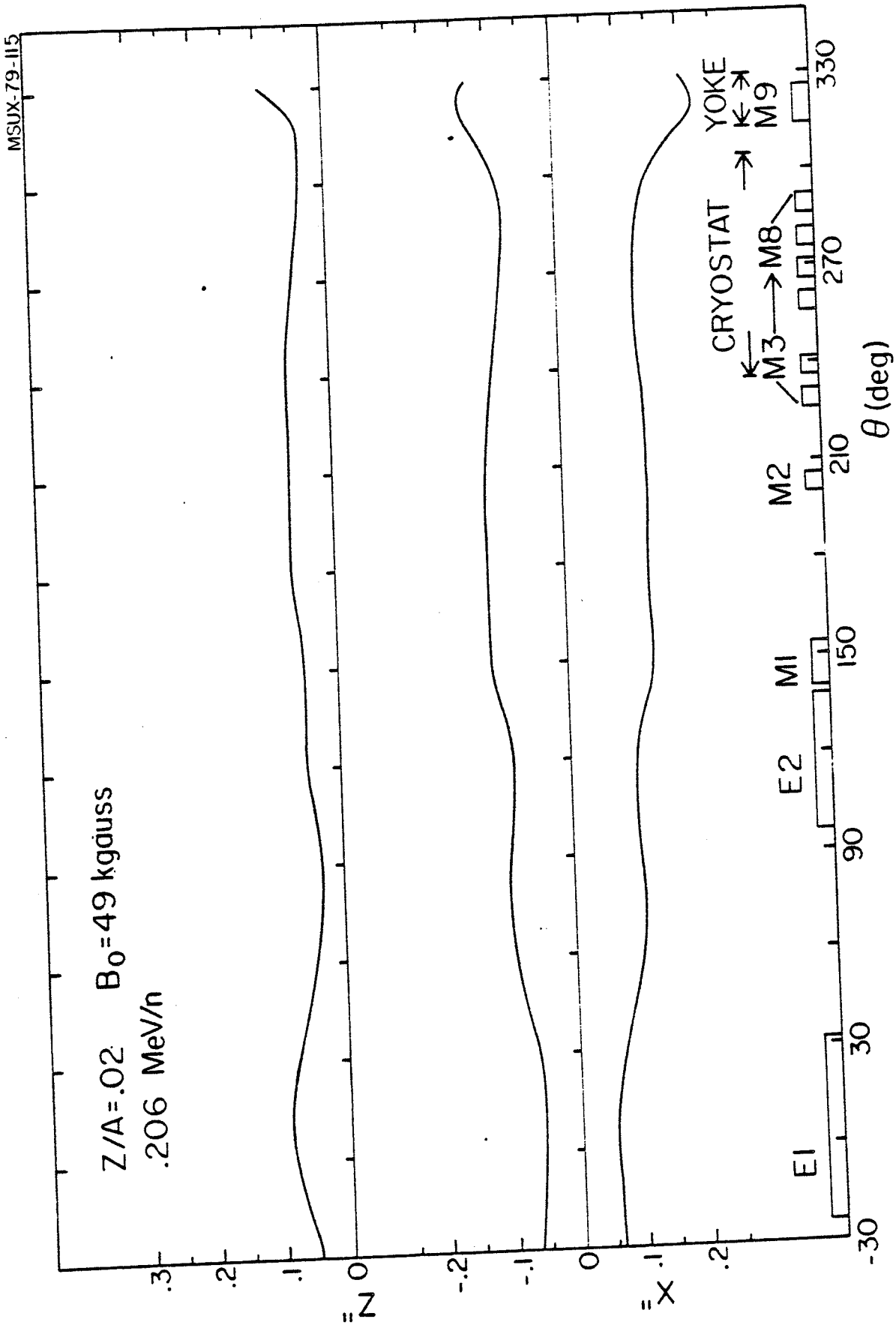

FIG. 15. Radial and axial beam envelopes along the extraction path for the ion with Z/A = .02 and B_o = 49 kgauss.

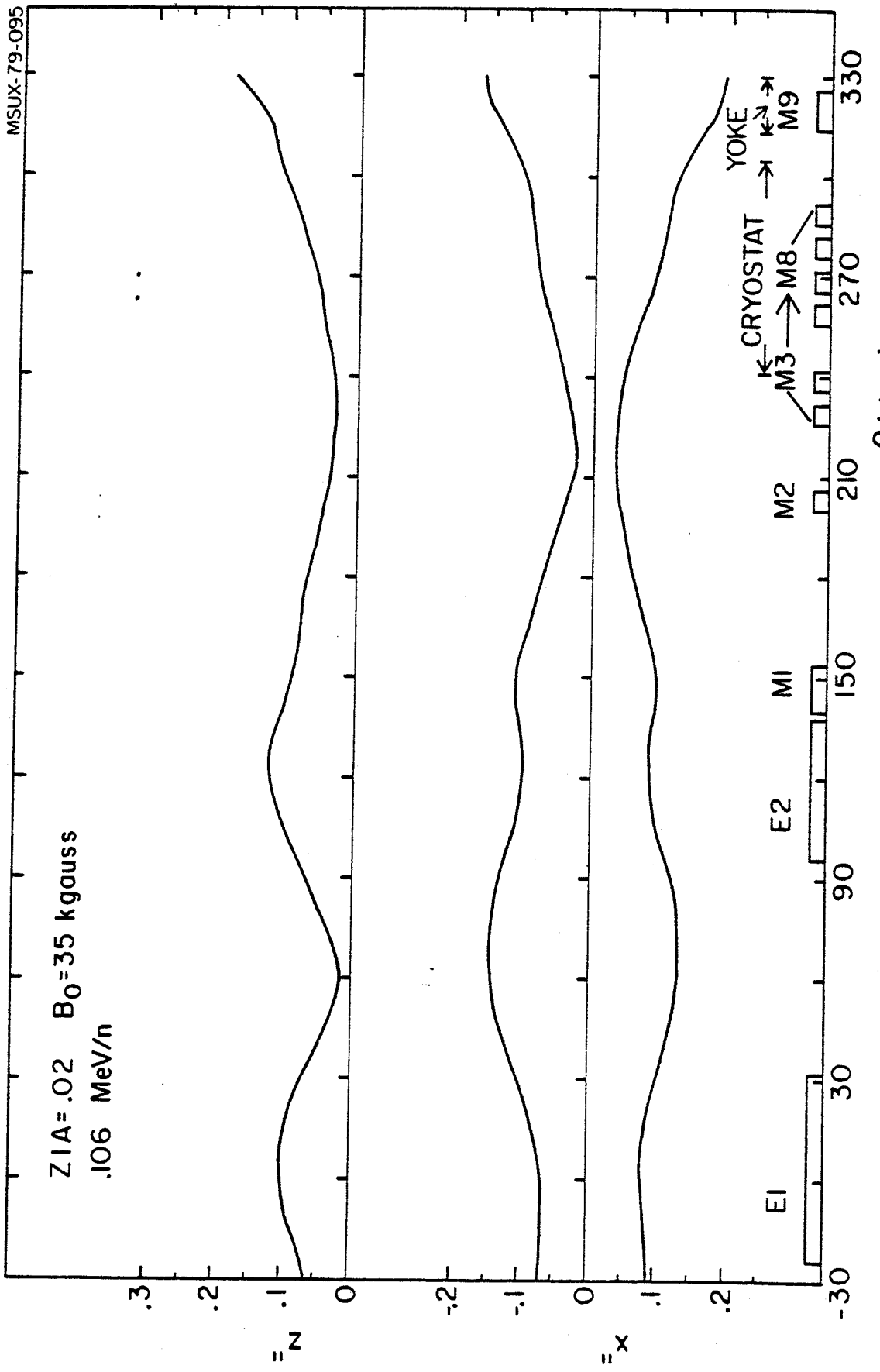

FIG. 16. Radial and axial beam envelopes along the extraction path for the ion with Z/A = .02 and Bo = 35 kgauss.

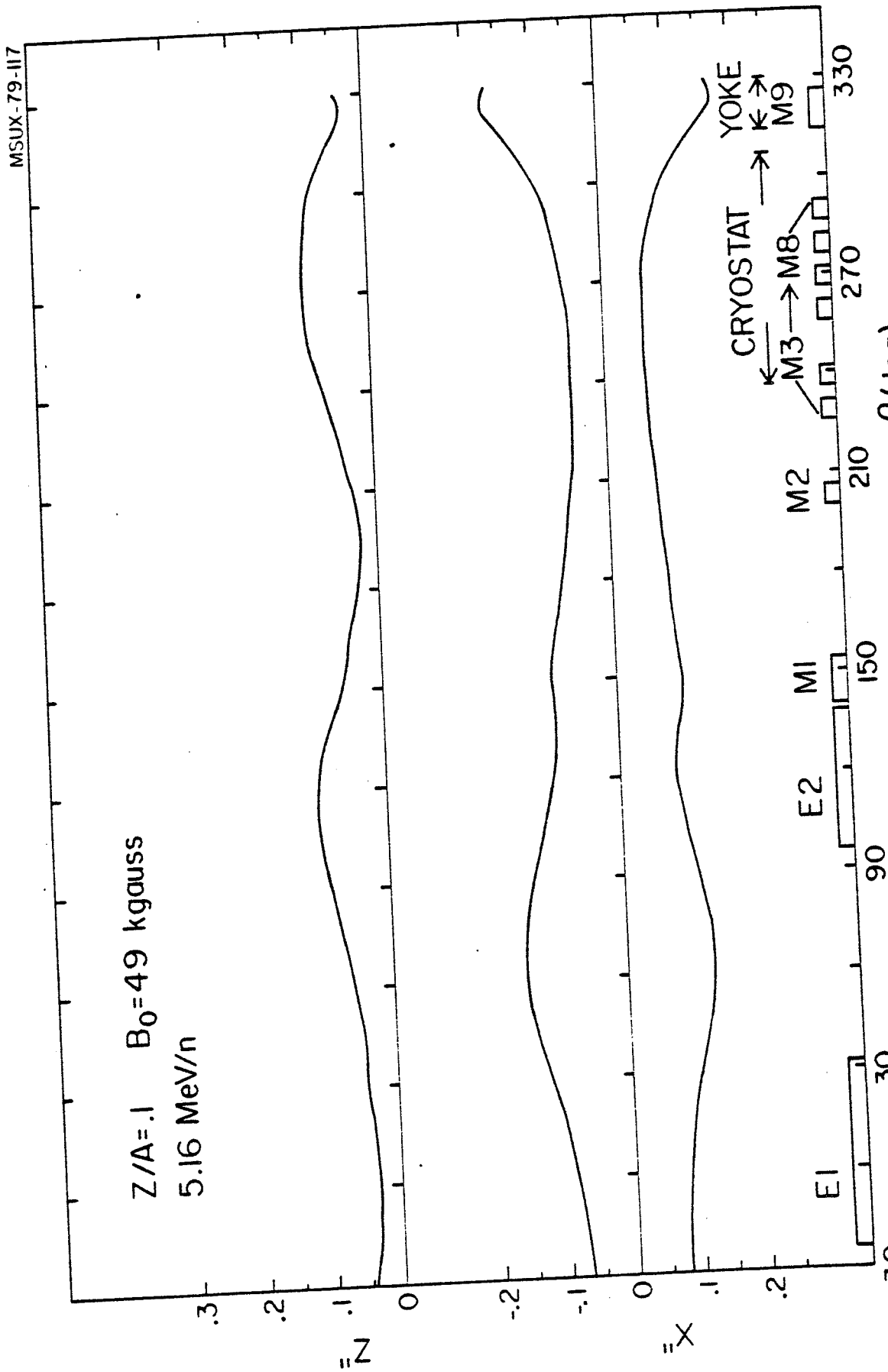

FIG. 17. Radial and axial beam envelopes along the extraction path for the ion with Z/A = .1 and B_o = 49 kgauss.

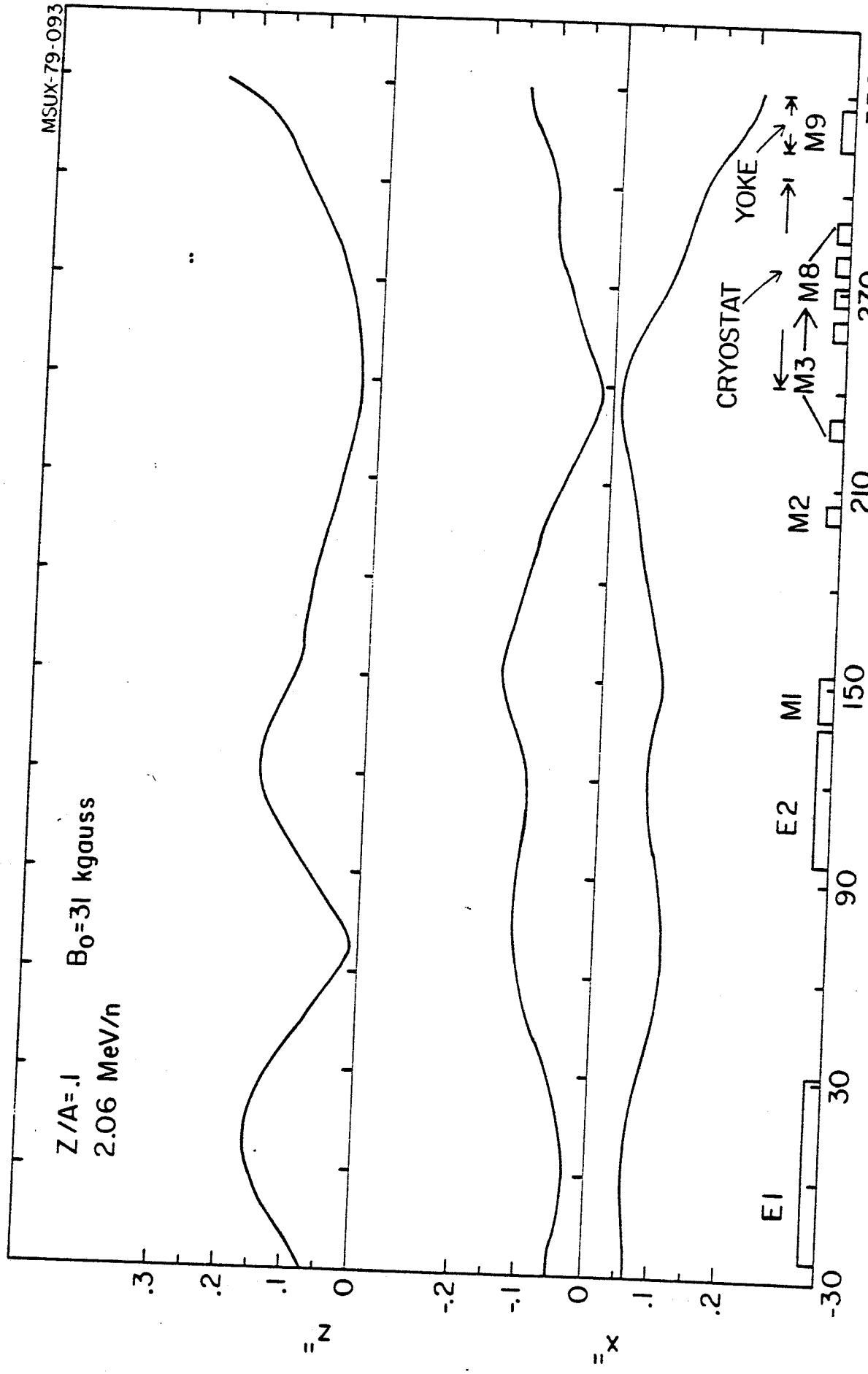

FIG. 18. Radial and axial beam envelopes along the extraction path for the ion with Z/A = .1 and B_o = 31 kgauss.

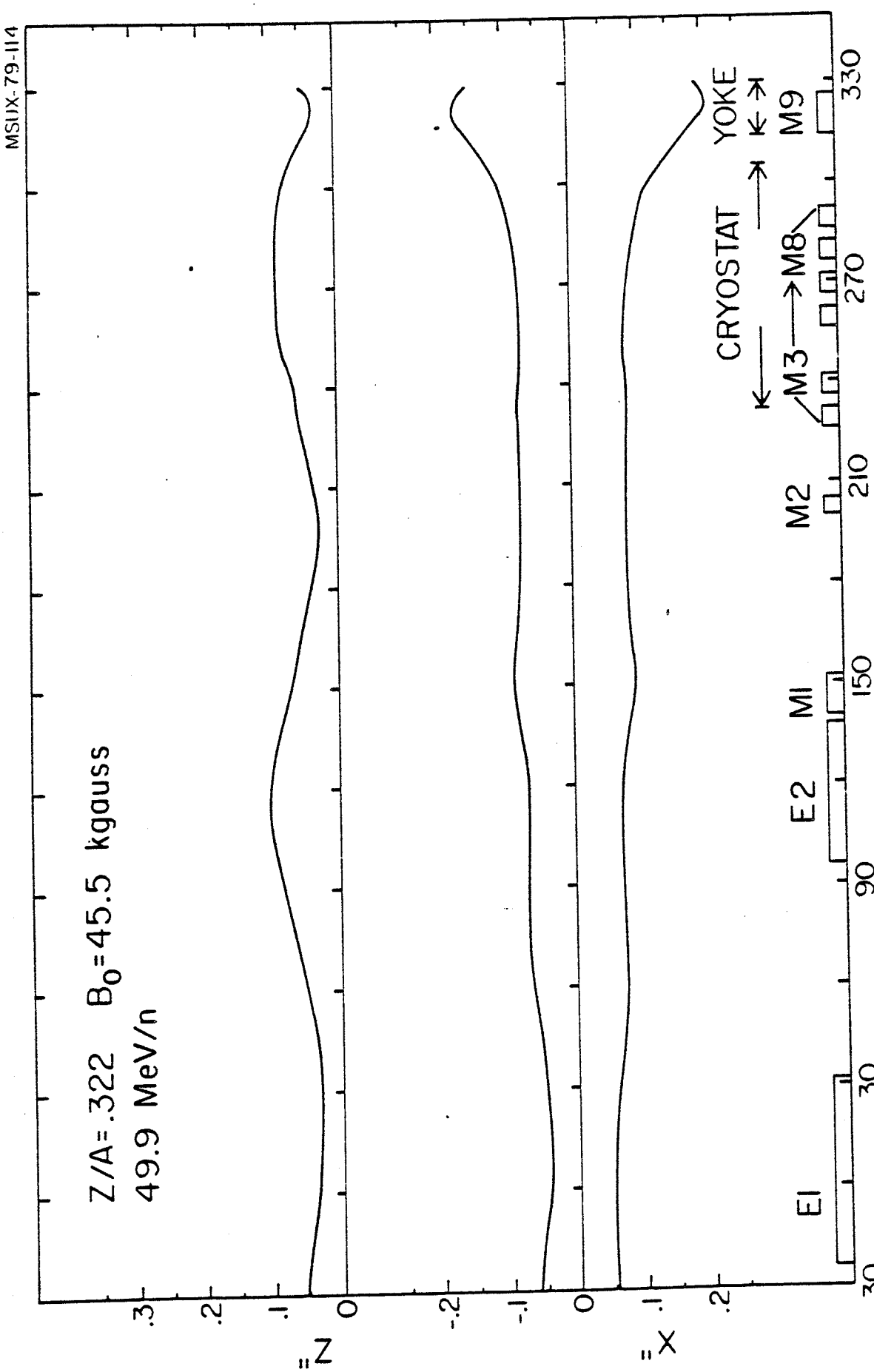

FIG. 19. Radial and axial beam envelopes along the extraction path for the ion with Z/A = .322 and B_0 = 45.5 kgauss.

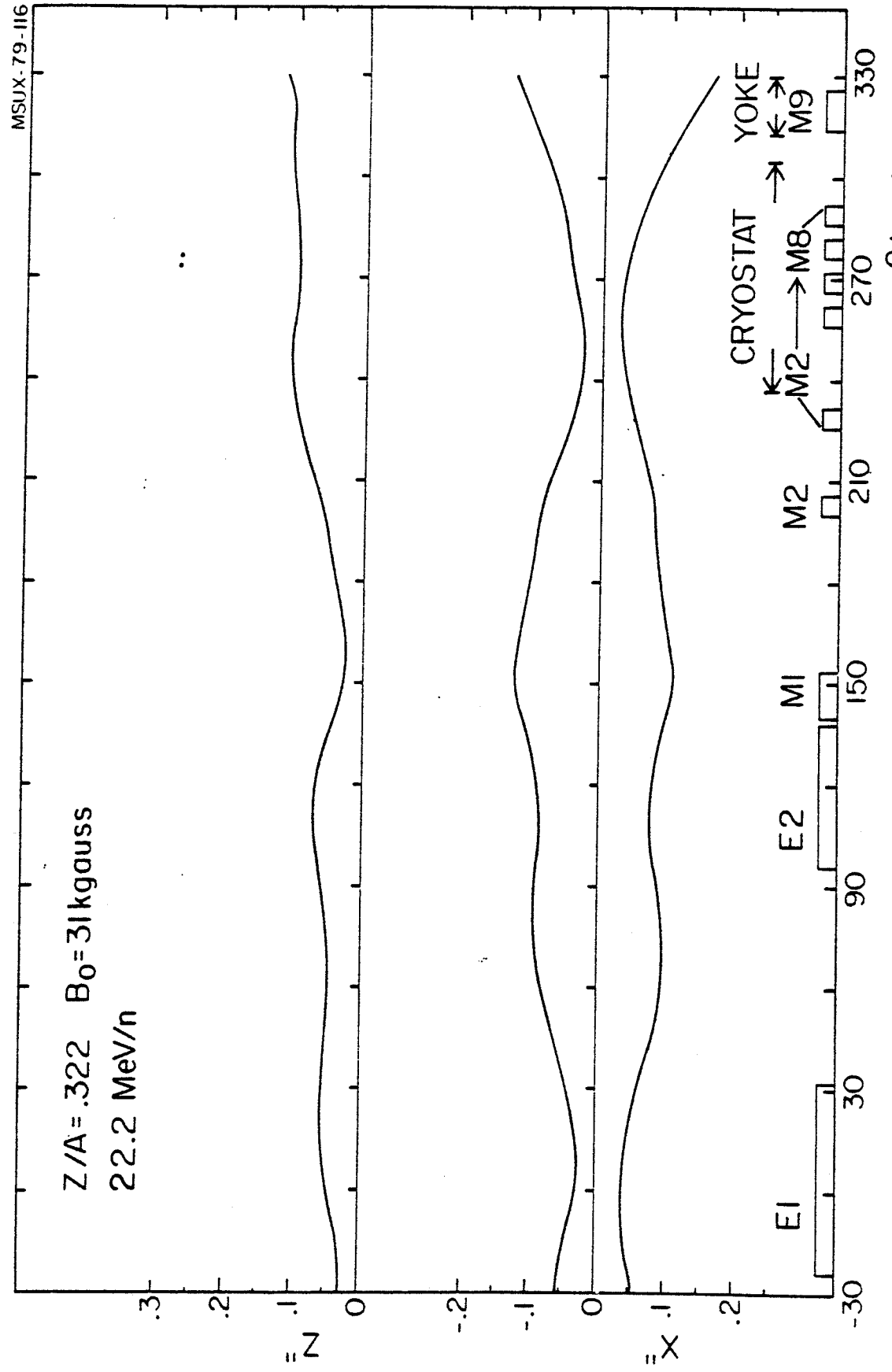

FIG. 20. Radial and axial beam envelopes along the extraction path for the ion with Z/A = .322 and B_o = 31 kgauss.

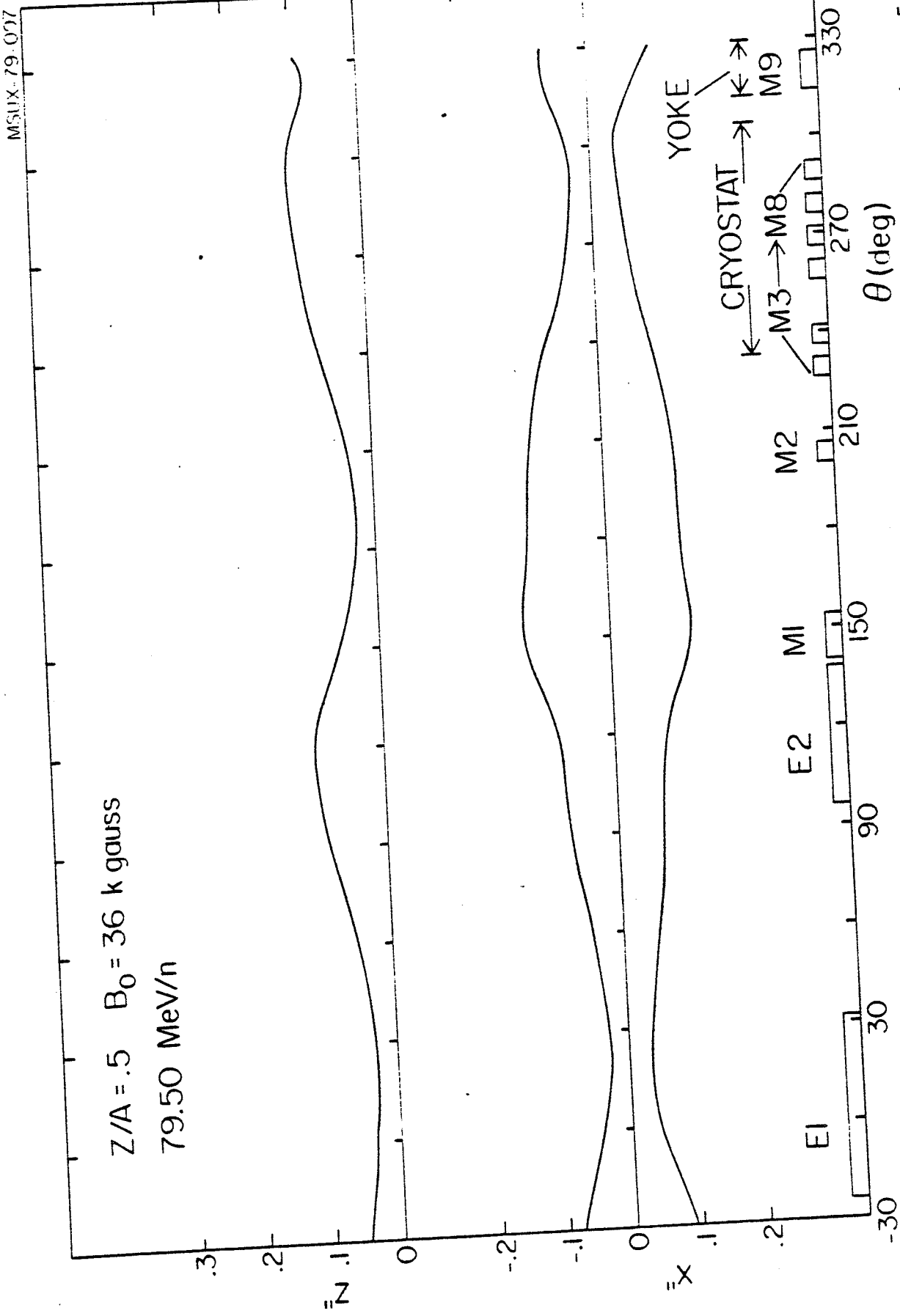

FIG. 21. Radial and axial beam envelopes along the extraction path for the ion with Z/A = .5 and B_o = 36 kgauss.

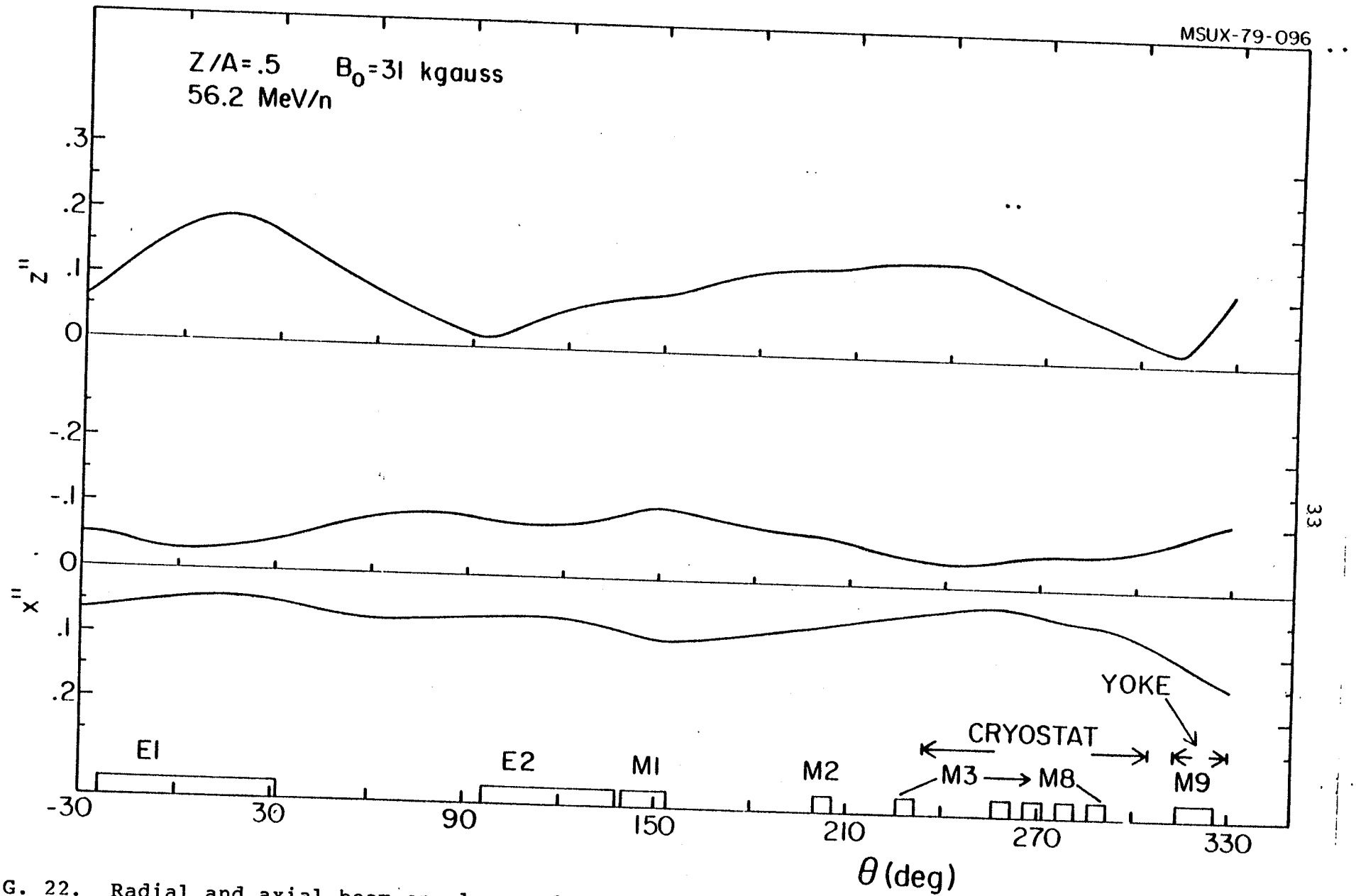

FIG. 22. Radial and axial beam envelopes along the extraction path for the ion with Z/A = .5 and B_o = 31 kgauss.

conditions for these beams have been determined by extensive beam dynamics calculations prior to extraction, and are reported in detail in [3]. Here we just recall that all beams exhibit a sufficient turn to turn spearation for clearing the septum, and that their emittance has been assumed as 6-7 mm mrad in both phase spaces.

All eight beams are well confined both radially and axially along the entire extraction path. In particular, the radial envelope is never larger than $\pm$ .15" around the central ray and in fact is at most $\pm$ .12" inside the electrostatic deflectors. This led to the present choice of 8 mm for the gap in the latter. It should be noted, as apparent from Figs. 18,20 and 22 that for the very low field cases, i.e. B_o=31 kgauss channel M_4 is not needed and is assumed to be removed. This is due to the fact that the saturated iron bars provide a focusing gradient that is independent from the main field level and the presence of M_4 resulted in a radial overfocusing for the ions with B_o=31 kgauss. In any case the need for removing M_4 does not appear until a center field value $B_o \simeq 33$ kgauss is reached, as the case of Z/A=.02 and B_o=35 kgauss shows.

The axial envelope shows some differences between the high and the low fields cases, the latter being typically less confined. This is due to differences in the starting conditions[3] again related to the presence of the $\nu_R + 2\nu_Z=3$ resonance, which tends to defocus the beam near the extraction radius.

The radial and axial phase spaces for all eight beams at $\theta=308^{o}$, R ≃ 40", are shown in Figs. 23 and 24 for the four injector-mode and the four stand-alone mode beams respectively. Distortions look very small, if not altogether negligible. It should be noted that for the radial emittance the ellipses have practically the same posture in the (x,p_x) plane, reflecting the very nearly constant ν_R values for all ions both at the extraction radius and along the extraction path. The axial phase-space instead changes considerably form one ion to the next, reflecting sizable differences in the ν_z values.

As a summary, the present extraction system seems quite adequate for the K-500 cyclotron, providing well confined beams throughout the operating range. We shall now turn to a discussion of the beam behavior in the traversal of the magnet yoke.

4. Yoke traversal

a-Phase space behaviour

The yoke extends from 42" to 60" in radius and the way it's crossed by the extracted beams is shown in Fig. 1. Since the trajectories in this region make an angle of 30^{o} with the radius, the path length through the yoke is roughly 25" long. It had been assumed that no further correcting elements would be needed in this region, and that quadrupoles placed sufficiently close to the cyclotron would be sufficient to handle the beams. This proved not to be the case.

Magnetic field measurements in the yoke hole provided for the extracted beams were carried out at several main coils

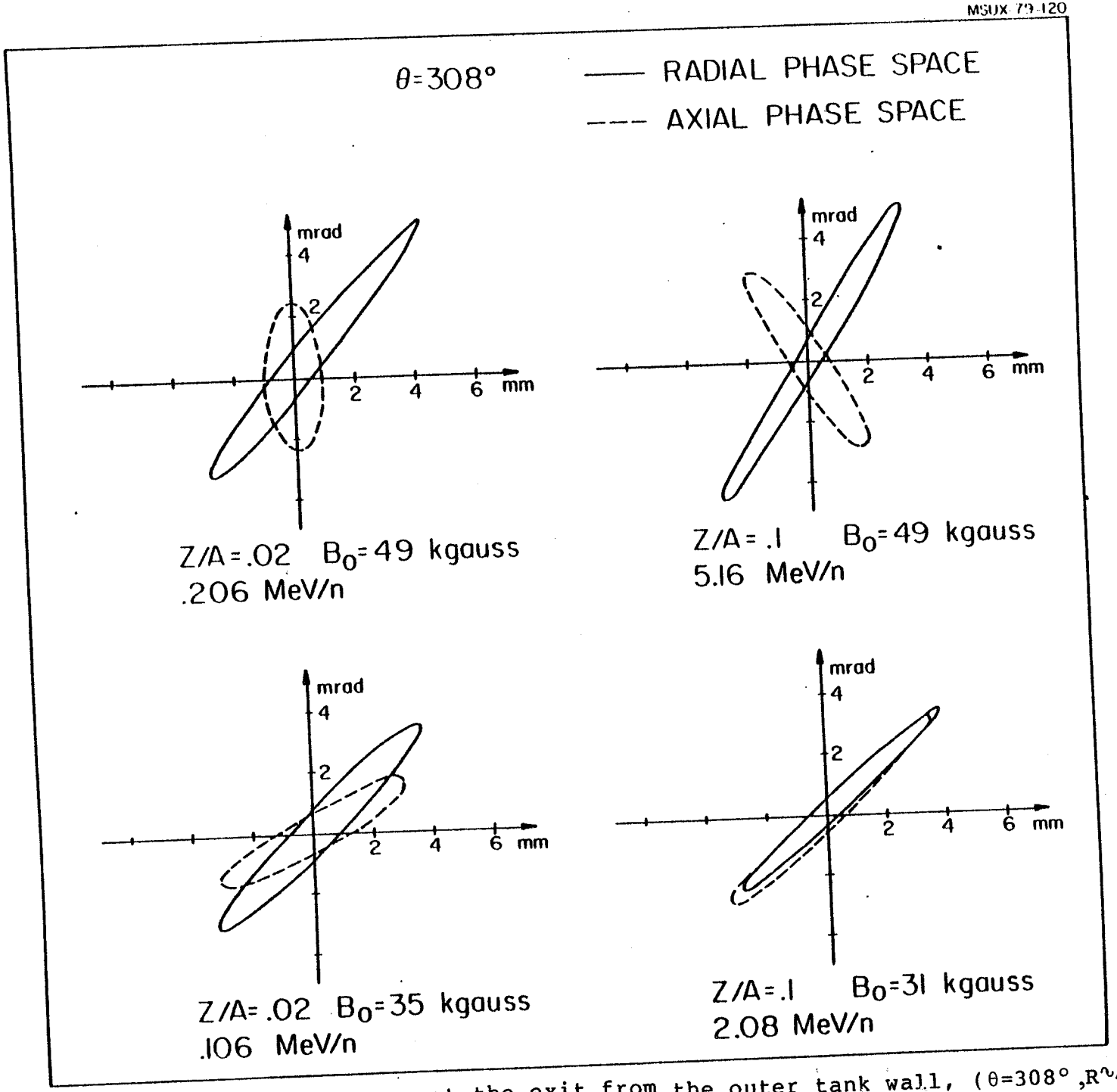

FIG. 23. Radial and axial phase spaces at the exit from the outer tank wall, (θ=308°, R$\sim$40") for four injector mode beams.

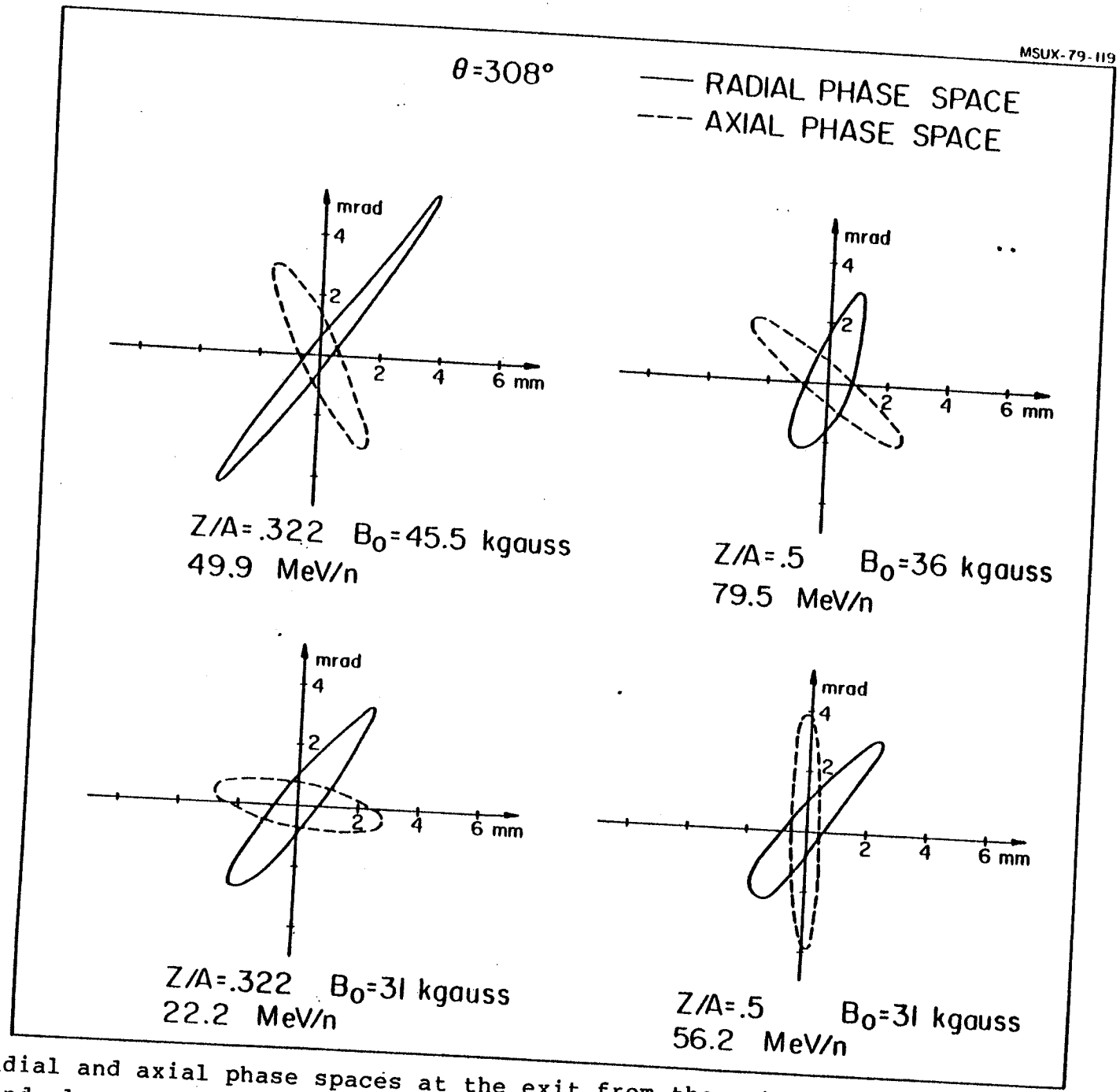

FIG. 24. Radial and axial phase spaces at the exit from the outer tank wall, (θ=308°,R$\sim$40") for four stand alone mode beams.

excitations. The results are shown in Fig. 25, the negative values implying a sign opposite to that of the internal field. The field is rather uniform over the 45" to 55" range, radial gradients existing at both ends as expected. The average field value in the uniform region can be plotted as a function of the sum of the coils currents, yielding an almost linear trend, as shown in Fig. 26. At the maximum excitation the field reaches about -6 kgauss, therefore giving a small effect of changing sign to the beams curvature.

Phase space tracking in the measured field yields results like those shown in Fig. 27 for the ion with Z/A = .322, B_o=45.5 kgauss. The radial phase space at R$\sim$40", discussed previously, is compared to the one at R$\sim$60", i.e. at the yoke exit. A defocusing effect is evident, the radial divergence almost doubling. The case presented here is the worst one, but similar results are observed for all other ions.

Although in principle these beams could be handled by quadrupoles close enough to the yoke exit, a radially focusing channel between 40" and 60" would certainly simplify problems.

Among the various options a passive channel looked as a very attractive one, especially if it could be made large enough so as to accomodate all beams. This feature would remove the need of moving radially the channel in order to position it along the different ions trajectories.

We succeeded in devising such a channel, whose cross section is shown in Fig. 28. Also shown are the gradient, $\frac{\partial B}{\partial x}$, and field bias - ΔB, which are expected in the hypothesis

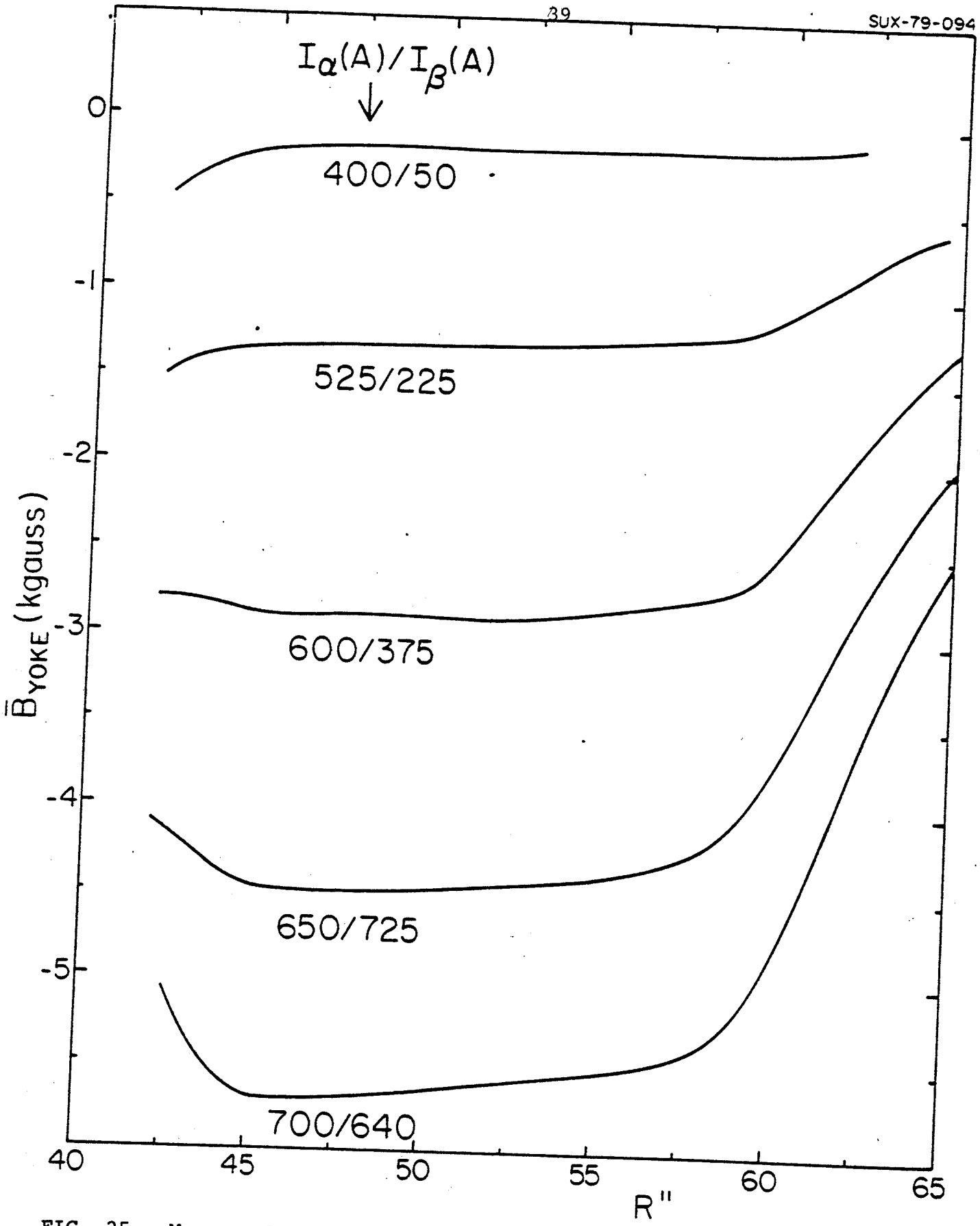

FIG. 25. Measured magnetic field in the yoke hole provided for extraction plotted as a function of the radius at different main coils excitations.

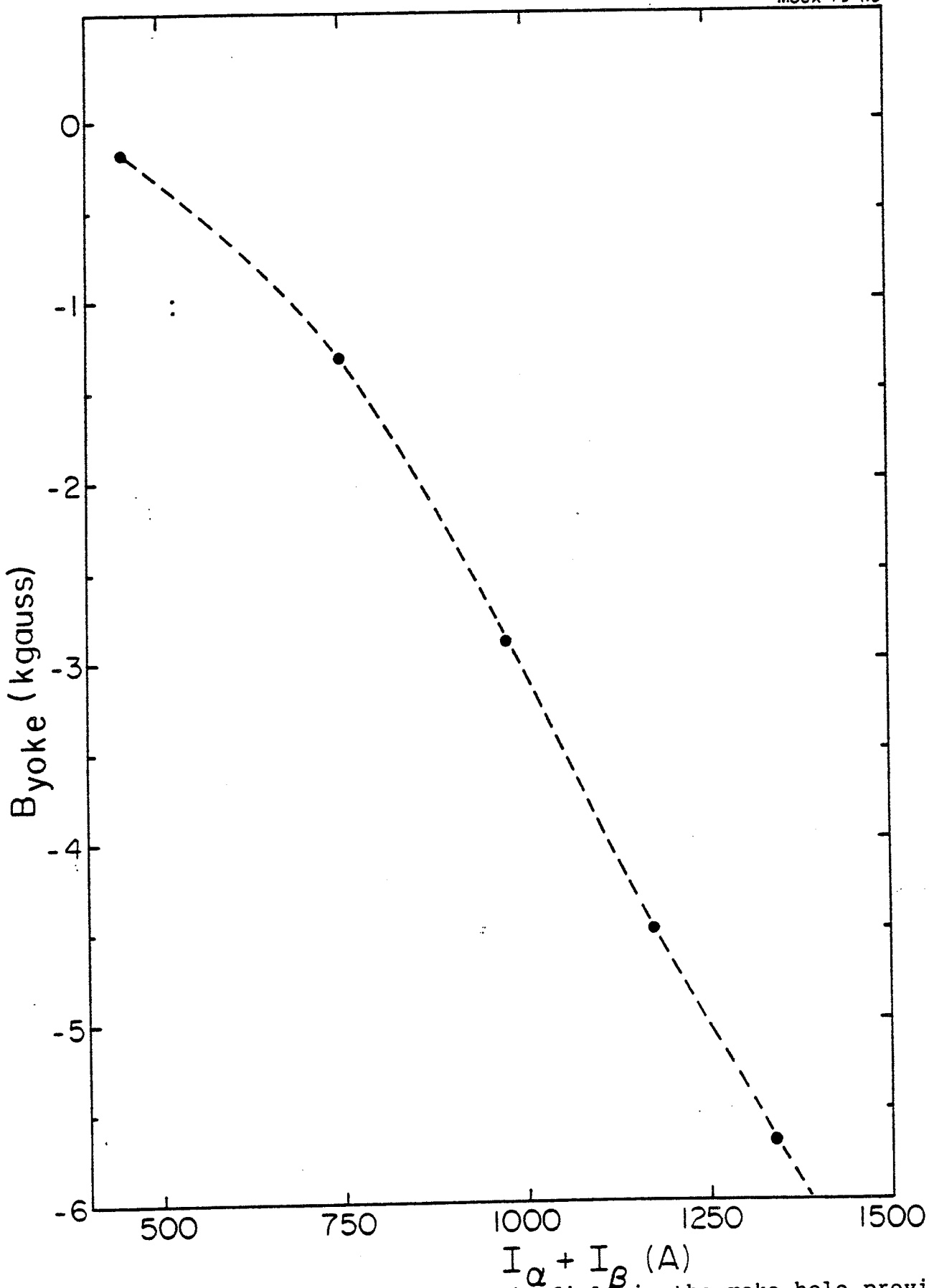

FIG. 26. Average value of the magnetic field in the yoke hole provided for extraction plotted as a function of the sum of the main coils currents.

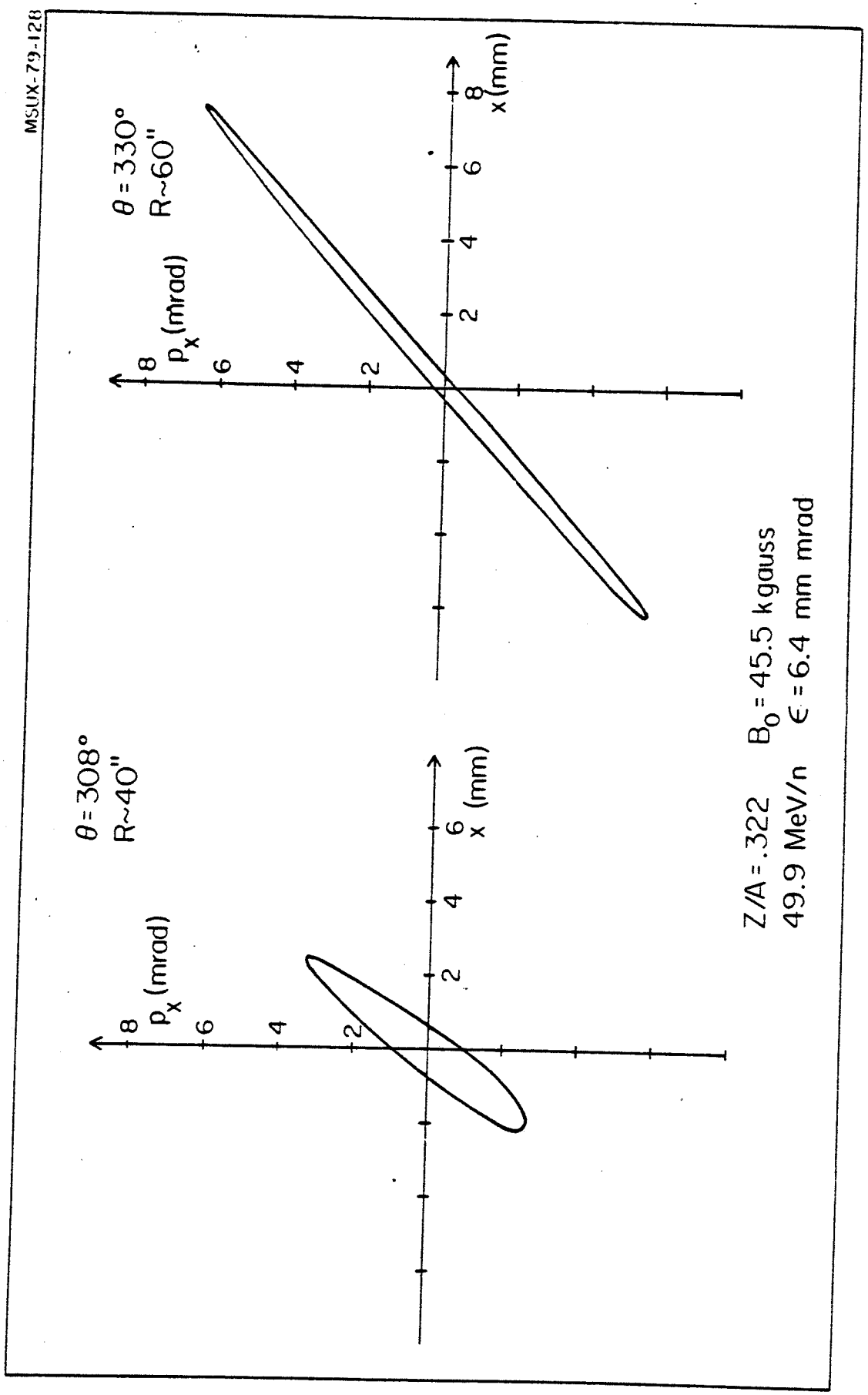

FIG. 27. Radial phase space at the entrance (left) and at the exit (right) from the yoke for the ion with Z/A=.322 and B_o =45.5 kgauss in the case of no magnetic channel inside the yoke.

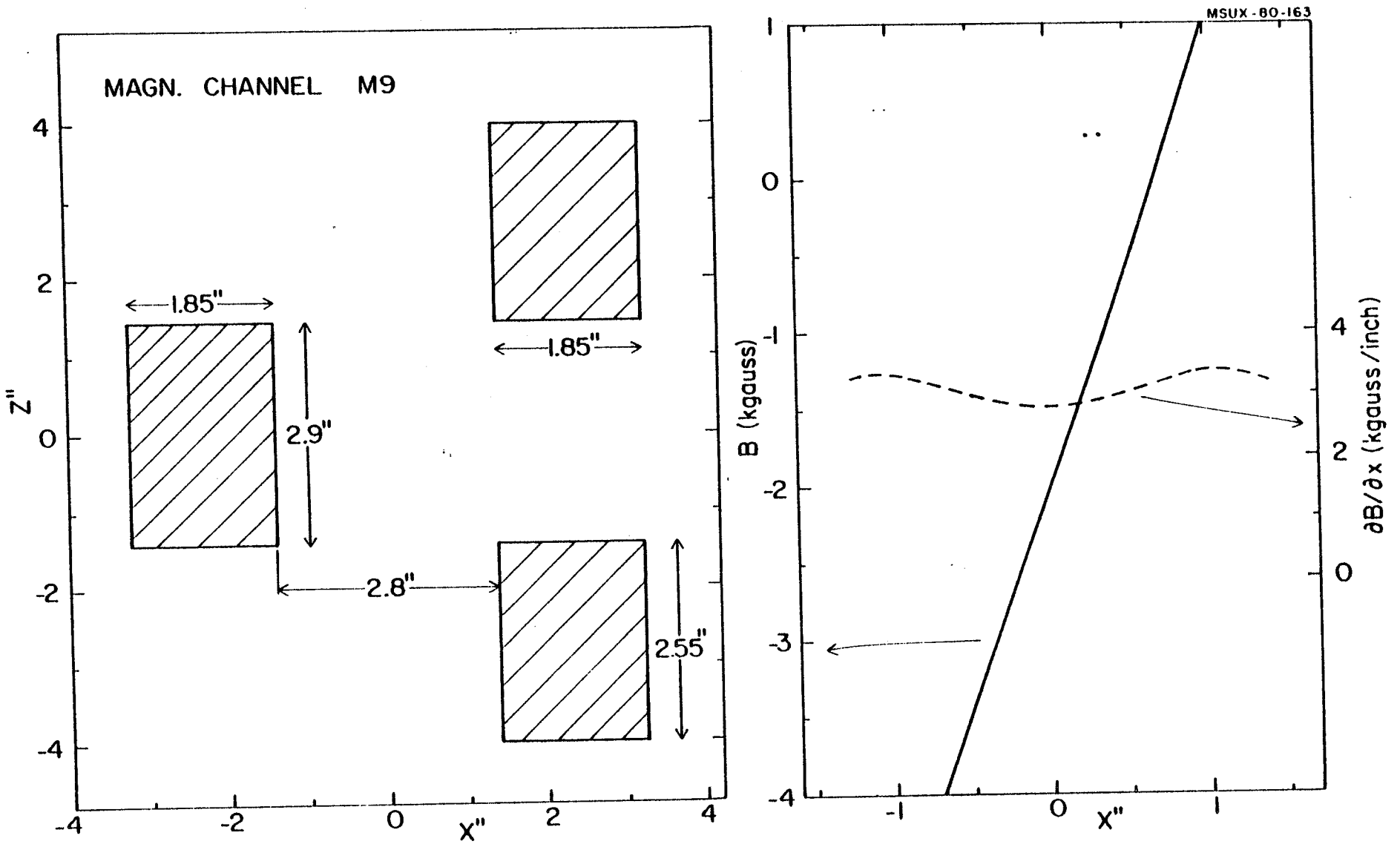

FIG. 28. Schematic cross section of the magnetic channel located in the yoke hole (left). The right side presents the field and the gradient across the channel, as calculated in the hypothesis of full saturation.

of full saturation. This channel provides therefore a rather uniform gradient of 3.1 kguass/inch over the radial range of $\pm$ 1.2".

The hypothesis of complete saturation does not hold, obviously, over the entire range of fields which are possible in the yoke hole. Calculations with the code TRIM[5] were therefore carried out, in order to find out the scaling law both of the gradient and of the field bias as a function of the strength of a superimposed field. The results are shown in Fig. 29 for the channel presented in Fig. 6 and prove that only at $B_{ext} \backsim$ 6 kgauss is the uniform saturation applicable. The gradient decreases by almost a factor of 3 if $B_{ext} \backsim$ 2 kgauss.

The field inside a magnetic channel similar to that of Fig. 28 and located in the exit hole of the yoke was measured at different main field levels. The results for the gradient are plotted in Fig. 30 as a function of the external field value and compared with TRIM predicitons. There is a very close agreement but it does not look like the iron bars are fully saturated yet at B_{ext}=6 kgauss.

These data were used in order to scale, according to the different main coils excitation levels, the gradient of the chosen channel shown in Fig. 28. A length of the channel of 15" has been selected, the channel thus extending between $\theta \backsim 317^{o}$ and $\theta \backsim 327^{o}$.

Phase space ellipses were then tracked through the yoke traversal path for all eight representative ions.

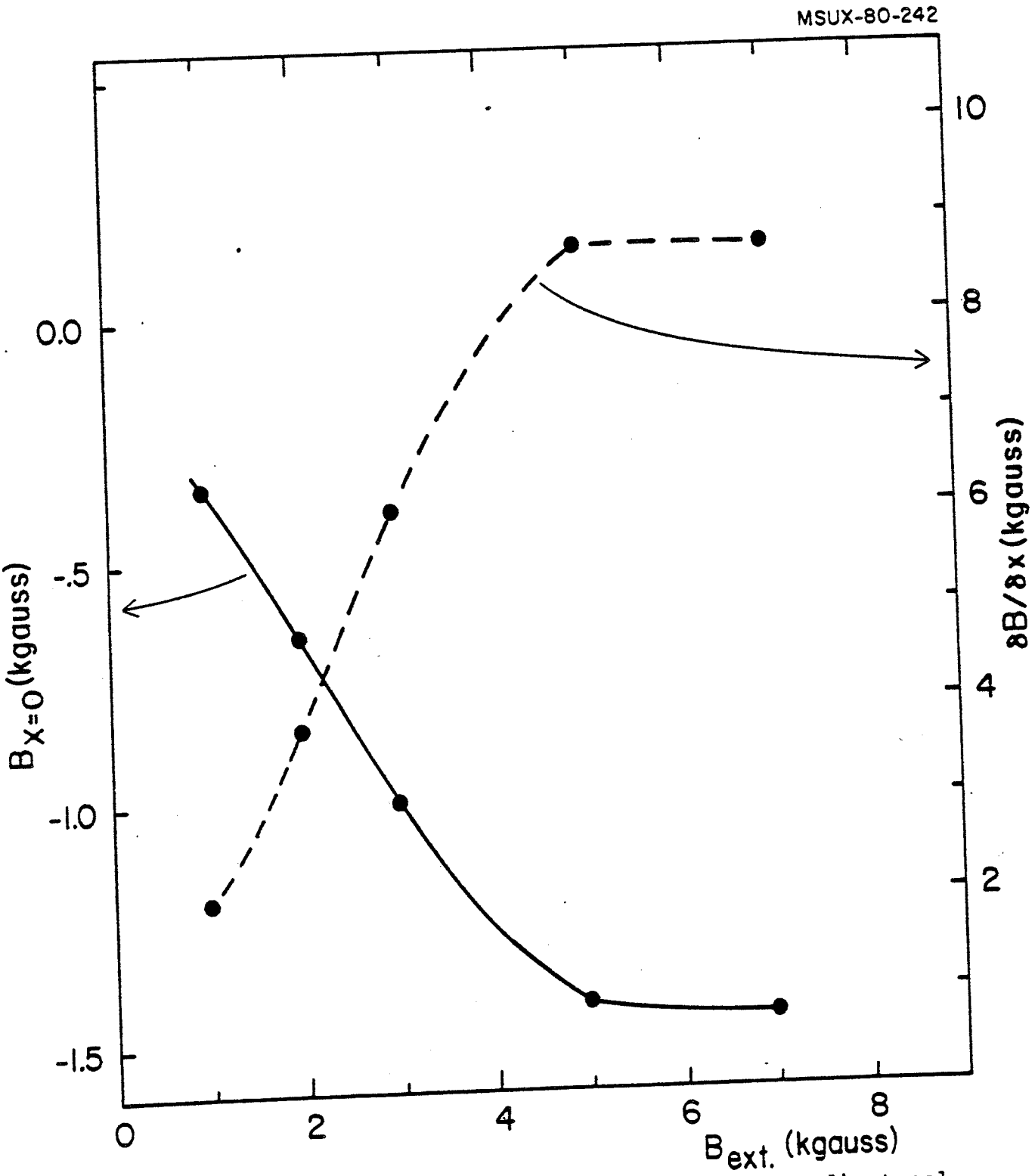

FIG. 29. Magnetic channel's center field and gradient calculated with the code TRIM plotted as a function of the external field. The channel geometry is that presented in Fig. 6.

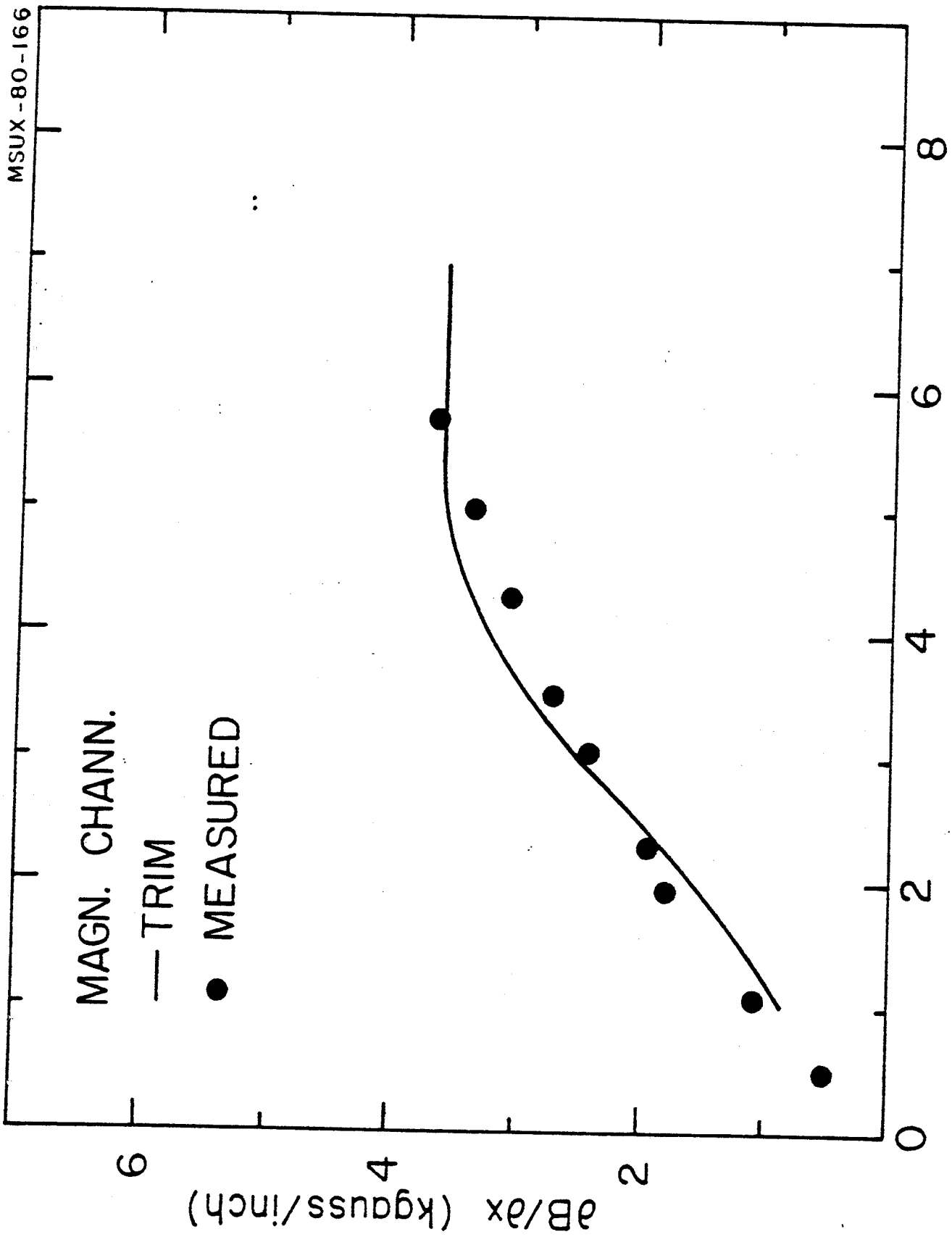

FIG. 30. Measured and calculated values of the gradients of the yoke magnetic channel plotted as a function of the external field.

The results, both for the axial and radial phase space, are presented in Figs. 31 and 32 for the injector and stand-alone beams respectively. These phase spaces are at $\theta = 330^{o}$, i.e. at approximately R=60" at the yoke exit. Given the relatively small divergences and beam sizes, and which do not pose any problem for the successive beam handling, this solution has been definitely adopted.

Table IV summarizes the data for the eight ions at $\theta = 330^{o}$ and $\theta = 334^{o}$. The scaled values of the channel gradient used in the calculations are listed.

Table IV. Central ray data at $\theta = 330^{o}$ and $\theta = 334^{o}$.

Z/A	B_o (kG)	T/A (MeV/n)	M_9 (kG/inch)	R"(330^{o})	R"(334^{o})	ϕ(334^{o})
.02	49.	.206	3.18	59.14	69.00	21.77^{o}
.02	35.	.106	1.53	60.29	69.00	25.14^{o}
.1	49.	5.16	3.17	59.00	69.00	21.45^{o}
.1	31.	2.08	.78	60.70	69.00	26.46^{o}
.322	45.5	49.87	3.0	59.05	69.00	21.64^{o}
.322	31.	22.20	1.04	60.50	69.00	25.83^{o}
.5	36.	79.05	1.99	59.73	69.00	23.54^{o}
.5	31.	56.17	1.15	60.44	69.00	25.61^{o}

All central rays can be made to pass at exactly the same point at R=69" and $\theta = 334^{o}$, i.e. a few inches outside the yoke exit (R=60"). At this point the central rays have a slightly variable angle with respect to the $\theta = 334^{o}$ radial line, denoted by ϕ in Table IV. The average value of this angle is $23.96^{o} \pm 2.5^{o}$.

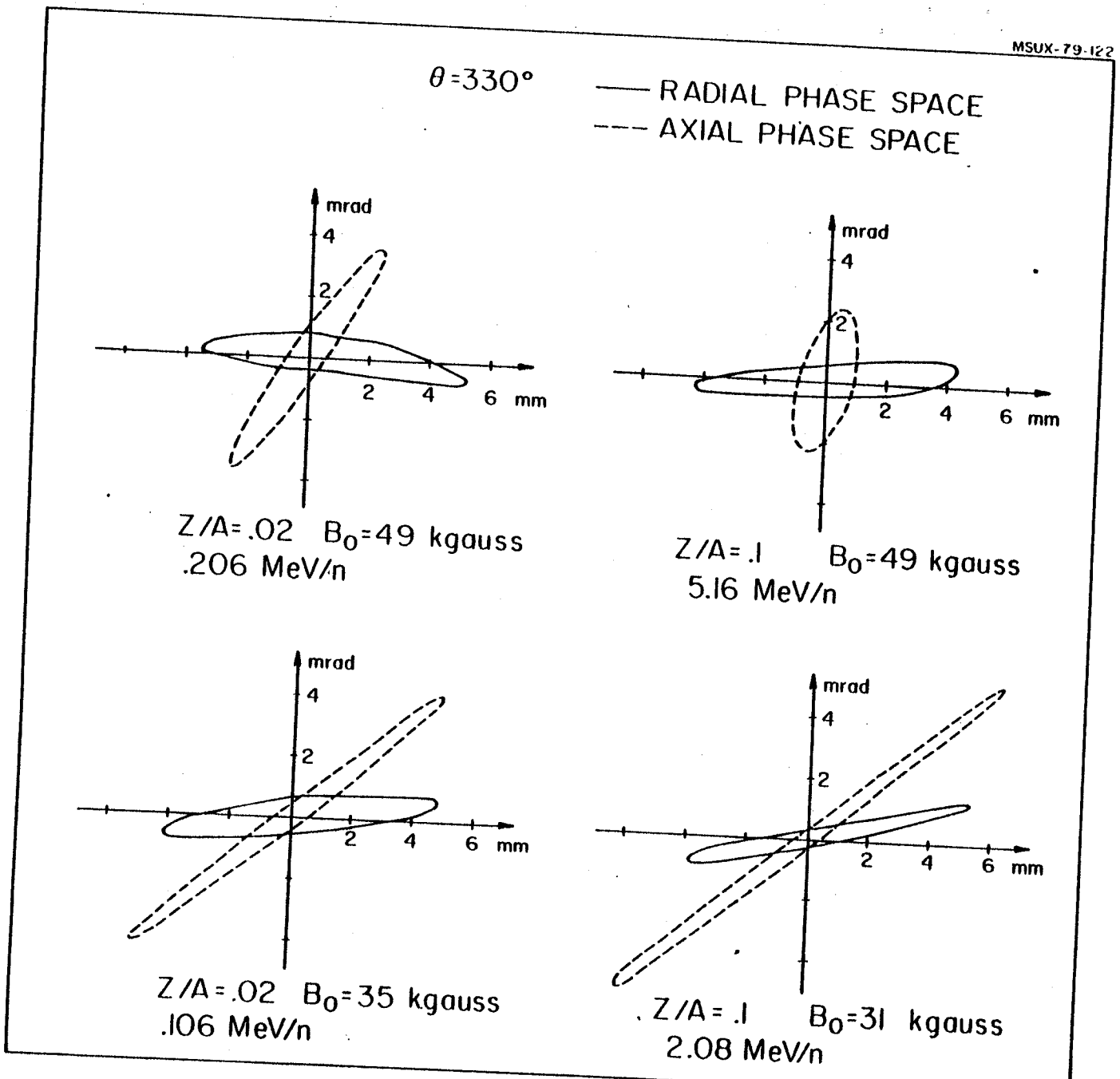

FIG. 31. Radial and axial phase space at the exit from the yoke (θ=330°, R∿60") for four injector mode beams.

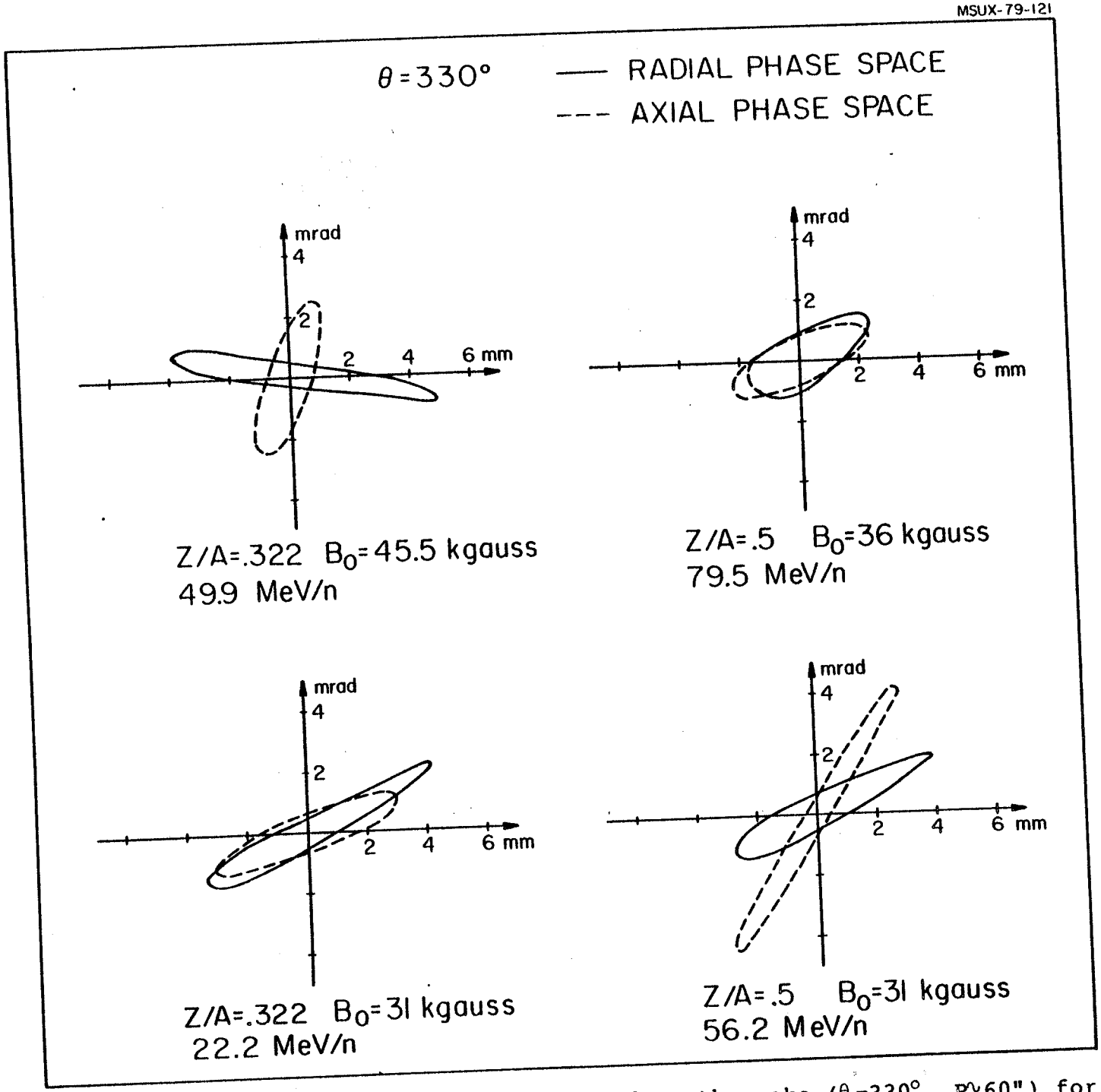

FIG. 32. Radial and axial phase space at the exit from the yoke (θ=330°, R$\sim$60") for four stand-alone beams.

Similar results would of course be obtained if the common point of all trajectories were chosen at some other distance from the yoke. As mentioned earlier this is accomplished by just varying the voltage of the second deflector. The usefulness of a common point for all beams is obviously that just one steering magnet at that point is needed to align all beams along the successive beam transfer line.

A schematic view of the envelope of all beams trajectories as they cross the yoke and through the channel M_9 is shown in Fig. 33, thus proving that the chosen channel does not need to be moved.

b-Dispersive effects

The radial and angular dispersion of the extracted beam generated by the energy spread in the beam itself must be known for the purpose of designing the beam transfer lines.

These effects have been therefore calculated, both with the channel in the yoke and without it. An example is presented in Fig. 34 for the ion with $Z/A=.02$ $B_o=49$ kgauss which is one of the most radially dispersive fields. The radial phase space ellipses corresponding to an energy spread $\frac{\Delta E}{E} = \pm .1\%$ are plotted for both cases. It is clear that the channel reduces dramatically the angular dispersion, and to some extent also the radial dispersion. The calculations are made by starting with the appropriate non-monochromatic phase space ellipses at the entrance of the first deflector, and are therefore fully consistent.

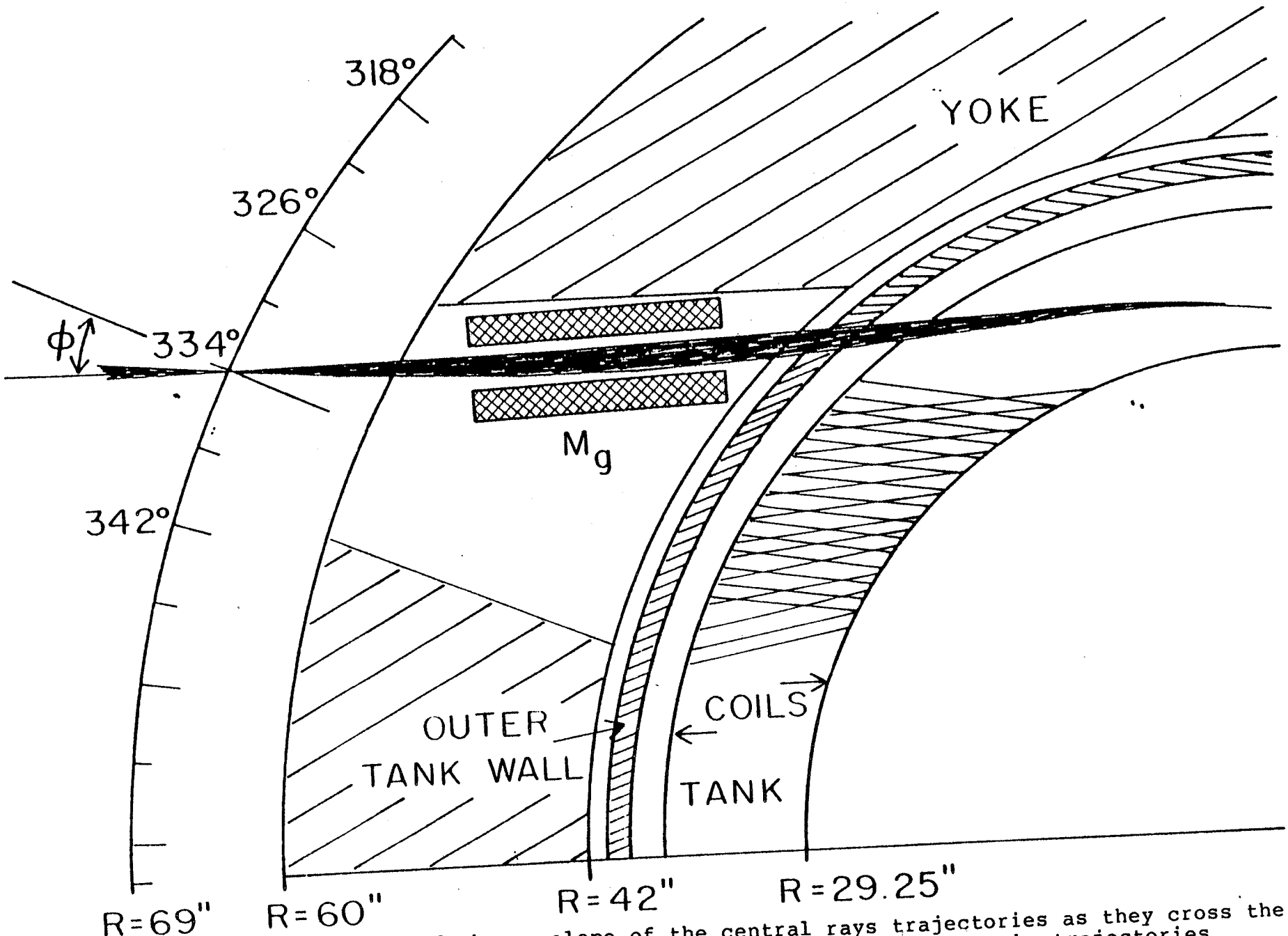

FIG. 33. Schematical view of the envelope of the central rays trajectories as they cross the yoke and through the channel M_g. Also shown are the common point of all the trajectories (R=69", θ=334°) and angle denoted as Φ in Table IV.

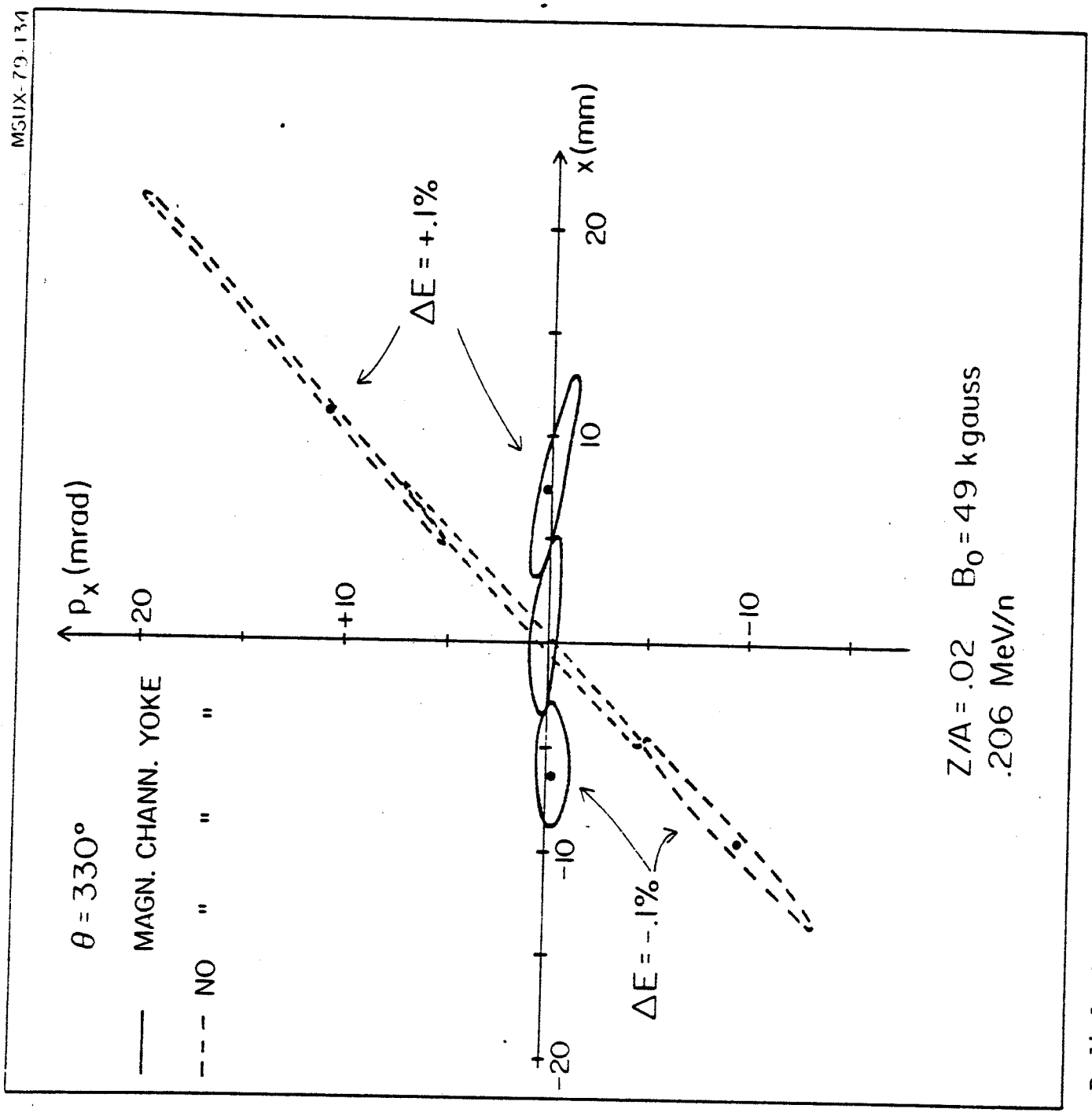

FIG. 34. Radial phase space at the exit from the yoke for the ellipses with an energy spread $\Delta E/E=0.$ and $\pm$ .1% for the ion with Z/A = .02 and B_o = 49 kgauss.

A summary of the dispersive effects for all eight ions is presented in Fig. 35 in terms of R_{16} and R_{26}, namely the radial and angular dispersions respectively, as defined in the beam transfer code TRANSPORT[6], i.e. cm (or mrad) per percent of momentum spread. The dashed area in the figure covers roughly the operating range of the K-500 cyclotron. It is of course possible to modify these contours if an active magnetic channel, instead of a passive one, is used. However, calculations with TRANSPORT show that there are no problems in handling these dispersions either for the purpose of an ordinary beam line or for the matching to the K-800 cyclotron when the K-500 is used in the injector mode[7]. The complication of an active channel does not seem therefore warranted at this stage.

5. Conclusions

The extraction system described here adequately fulfills all the requirements set forth for the K-500 cyclotron. Electric fields in the deflectors are not too high and in any case similar to those encountered in conventional AVF cyclotrons. The passive magnetic channels, although operating with a fixed gradient, are quite sufficient for beam focusing. Moreover their perturbations on the field, in terms of first and second harmonics, can be compensated with just two elements, that is a very small additional complication for this system.

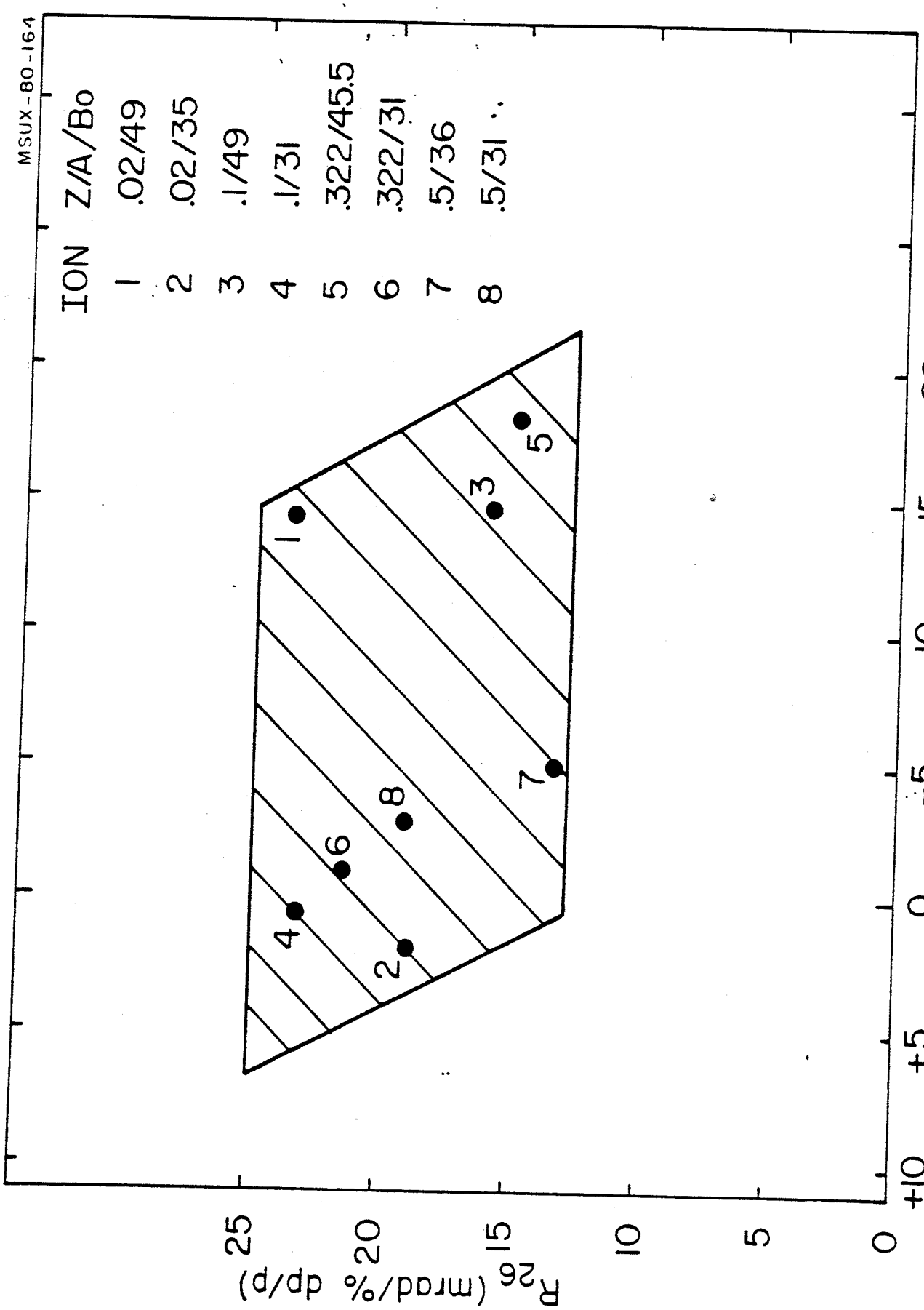

FIG. 35. Dispersive effects in terms of radial dispersion (R_{16}) and angular dispersion (R_{26}) for the eight listed ions. The dashed area roughly covers the operating range of the K-500 cyclotron.

Radial movability of every element within a range of $\pm$ .25" has been found essential. As discussed above, movability is rather important when a large number of elements is involved.

The need for an extra focusing channel in the yoke has been recognized and a passive channel seems so far an adequate solution. However, should an active channel be needed for the purpose of a better control of the phase space and dispersion characteristics of the external beams, it could be inserted later with really no difficulty.

Since the present design of the extraction system is based on measured fields or otherwise very realistic data no changes are anticipated until the initial operation of the cyclotron.

REFERENCES

1. M.M. Gordon, E.M. Fabrici, Beam Extraction System for the K=500 Superconducting Cyclotron, IEEE Transactions on Nuclear Science, NS26 (1979) 2101.
2. G. Bellomo, F. Resmini; Trimming of the Magnetic Field for the K-500 Cyclotron at MSU, to be published.
3. E. Fabrici, F.G. Resmini, A Survey of Beam Dynamics prior to extraction in the K-500 Cyclotron at MSU, to be published.
4. F. Resmini, G. Bellomo, E. Fabrici, H.G. Blosser, D. Johnson, Design Characteristics of the K=800 Superconducting Cyclotron at MSU, IEEE TRansactions on Nuclear Science, NS26 (1979) 2078.
5. J.S. Colonias; TRIM: A Magnetstatic Computer Program for the CDC 6600, UCRL-18439 (1968).
6. C.H. Moore, S.K. Howry, H.S. Butler; TRANSPORT, A Computer Program for Designing Beam Transport Systems. Stanford University (1964).
7. K-800 Conceptual Report; MSUCL-282 (Dec. 1978).